mRNA delivery of genetically encoded mosaic-8 pan-sarbecovirus RBD vaccines

Alexander A. Cohen[1], Jennifer R. Keeffe[1], Lusineh Manasyan[1], Indeever Madireddy[1], Ange-Célia I. Priso Fils[1], Kim-Marie A. Dam[2], Haley E. Stober[2], Rory A. Hills[3,4,7], Woohyun J. Moon[5], Paulo J.C. Lin[5], Mark R. Howarth[3], Magnus A.G. Hoffmann[2,6,8*], Pamela J. Bjorkman[1,8*]

Affiliations

[1]Division of Biology and Biological Engineering, California Institute of Technology, Pasadena, CA 91125, USA

[2]Gladstone Institutes, San Francisco, CA 94158, USA

[3]Department of Pharmacology, University of Cambridge, Tennis Court Road, Cambridge, CB2 1PD, UK

[4]Department of Biochemistry, University of Oxford, Oxford, OX1 3QU, UK

[5]Acuitas Therapeutics, Vancouver, BC, V6T 1Z3, Canada

[6]Department of Medicine, University of California, San Francisco, CA 94143, USA

[7]Present address: Department of Pathology, Stanford University, School of Medicine, Palo Alto, CA 94305, USA

[8]Lead contact

[*]Correspondence: magnus.hoffmann@gladstone.ucsf.edu, bjorkman@caltech.edu

Keywords

Deep mutational scanning; epitope mapping; mRNA and protein nanoparticle vaccines; pandemic preparedness; pan-sarbecovirus vaccine; systems serology; SySPEM (systems serology-polyclonal epitope mapping)

Summary

Global health remains threatened by spillovers of zoonotic SARS-like betacoronaviruses (sarbecoviruses) that could be mitigated by a pan-sarbecovirus vaccine[1]. We described elicitation of potently neutralizing and cross-reactive anti-sarbecovirus antibodies by mosaic-8 nanoparticles (NPs) displaying eight different sarbecovirus spike receptor-binding domains (RBDs) as 60 copies of eight individual RBDs[2-6] (mosaic-8 RBD-NPs) or 30 copies of two "quartets," each presenting four tandemly-arranged RBDs[7] (dual quartet RBD-NPs). To facilitate manufacture of a broadly protective mosaic-8 vaccine, we generated membrane-bound RBD quartets that can be genetically encoded and delivered via mRNA: dual quartet RBD-mRNA and dual quartet RBD-EABR-mRNA, which utilizes ESCRT- and ALIX-binding region (EABR) technology that promotes immunogen presentation on cell surfaces and circulating enveloped virus-like particles (eVLPs)[8]. Immunization with mRNA immunogens elicited equivalent or improved binding breadths, neutralization potencies, T cell responses, and targeting of conserved RBD epitopes across sarbecoviruses, demonstrating successful conversion of protein-based mosaic-8 RBD vaccines to mRNA formats. Systems serology[9] showed that the mRNA vaccines elicited balanced IgG subclass responses with increased Fcγ receptor-binding IgGs, consistent with potentially superior Fc effector functions. A new technique, Systems Serology-Polyclonal Epitope Mapping (SySPEM), revealed distinct IgG-subclass-specific epitope targeting signatures across mRNA and protein-based vaccine modalities. These results demonstrate successful conversion of mosaic-8 RBD-NPs to mRNA or EABR-mRNA vaccines that provide easy manufacturing and enhanced protection from future pandemic sarbecovirus outbreaks.

Introduction

Three coronaviruses have spilled over from animal hosts to cause human epidemics or pandemics in the past 25 years: SARS-CoV (hereafter SARS-1) in the early 2000s, MERS-CoV in 2012, and SARS-CoV-2 (hereafter SARS-2) in 2019[10]. Two of these coronaviruses, SARS-1 and SARS-2, are members of the SARS-like betacoronavirus (sarbecovirus) subgenus. Although SARS-1 is not currently circulating, SARS-2 continues to infect humans, driving emergence of new variants that necessitate regular updates of current COVID-19 vaccines[11]. Since we cannot predict how SARS-2 will continue to mutate or which zoonotic sarbecovirus will next infect humans, we need a pan-sarbecovirus vaccine that does not need updating to provide broad protection against new SARS-2 variants and future sarbecovirus spillovers[1].

Spike trimers of coronaviruses function in host cell entry after one or more of the receptor-binding domains (RBDs) adopt an "up" position to permit interactions with a host cell receptor[12]. RBD targeting has been suggested for COVID-19 vaccine development as RBDs are the main target of neutralizing antibodies (Abs)[13]. We previously described a vaccine approach designed to elicit broad Ab responses to diverse sarbecoviruses in which RBDs from multiple sarbecoviruses were covalently linked using the SpyCatcher-SpyTag system[2-5] to a SpyCatcher-mi3 protein nanoparticle[14] (NP)[2-5]. In this approach, mosaic-8 RBD-NPs displayed eight different sarbecovirus spike RBD antigens attached randomly to the 60 positions of the mi3 NP (Fig. 1a,b). We hypothesized that B cells bearing cross-reactive receptors (B cell receptors; BCRs) recognizing features in common between adjacent non-identical RBDs would be preferentially activated compared to B cells with BCRs recognizing immunodominant strain-specific epitopes[3] (Fig. 1a). To investigate this prediction, we used deep mutational scanning (DMS)[15] to map RBD epitopes recognized by Abs from animals immunized with mosaic-8 RBD-NPs or homotypic RBD-NPs (i.e., only presenting SARS-2 RBD), which revealed targeting of more conserved RBD regions by mosaic-8 RBD-NP–elicited Abs compared with targeting of more variable RBD regions by homotypic RBD-NP–elicited Abs[3-7]. This finding rationalized results from challenge experiments in which mosaic-8 RBD-NPs protected from both a matched viral challenge (i.e., from a virus represented by an RBD on the NP) and a mismatched challenge (i.e., from a virus not represented by an RBD on the NP), whereas homotypic RBD-NPs protected only from a matched challenge[3]. In addition to initial experiments in SARS-2–naïve animals, we also found broader Ab responses elicited by mosaic-8 RBD-NPs in animals that were pre-vaccinated with COVID-19 vaccines[4]. Taken together, these results suggest that a mosaic-8 RBD-based vaccine given as a COVID-19 booster could provide increased protection from SARS-2 variants and prevent future sarbecovirus spillover(s) from causing an epidemic or pandemic.

Manufacturing of a mosaic-8 RBD-NP vaccine is a challenging process that requires production of nine protein components: eight different RBDs and a NP to which the RBDs are coupled. Making an mRNA-based version of a mosaic-8 vaccine would also pose challenges due to the requirement of synthesizing eight individual modified mRNAs. The RBD-encoding mRNAs could either be packaged into individual lipid nanoparticles (LNPs) or co-formulated into a single LNP. In the first case, some cells would not take up all eight mRNA LNPs, therefore presenting fewer instances of different RBDs adjacent to each other, potentially reducing the hypothesized avidity effects to activate B cells with maximally cross-reactive BCRs (Fig. 1a). In the second case, co-formulation of eight mRNAs encoding each RBD into a single LNP would present technical and regulatory challenges. A potential solution relevant to converting a mosaic-8 vaccine into an mRNA format involves the reported modification of the mosaic-8 RBD-NP protein-based immunogen into an mi3 NP presenting two RBD "quartets" (each containing four RBDs arranged in tandem), which was shown to elicit equally broad and potent Abs as the original mosaic-8 RBD-

NP that presents monomeric RBDs[7] (Fig. 1c; dual quartet RBD-NP). Dual quartet RBD-NPs require manufacture of only three components (two RBD quartets and a NP), and by synthesizing mRNAs encoding membrane-bound RBD quartets, could be more easily converted to an mRNA-LNP format than mosaic-8 RBD-NPs. In addition to simpler manufacturing, mRNA-LNP vaccines offer an advantage over protein-based vaccines in that viral antigens undergo translation in the cytoplasm, thereby providing a source of viral peptides for presentation by MHC class I molecules to activate CD8+ cytotoxic T cells[16].

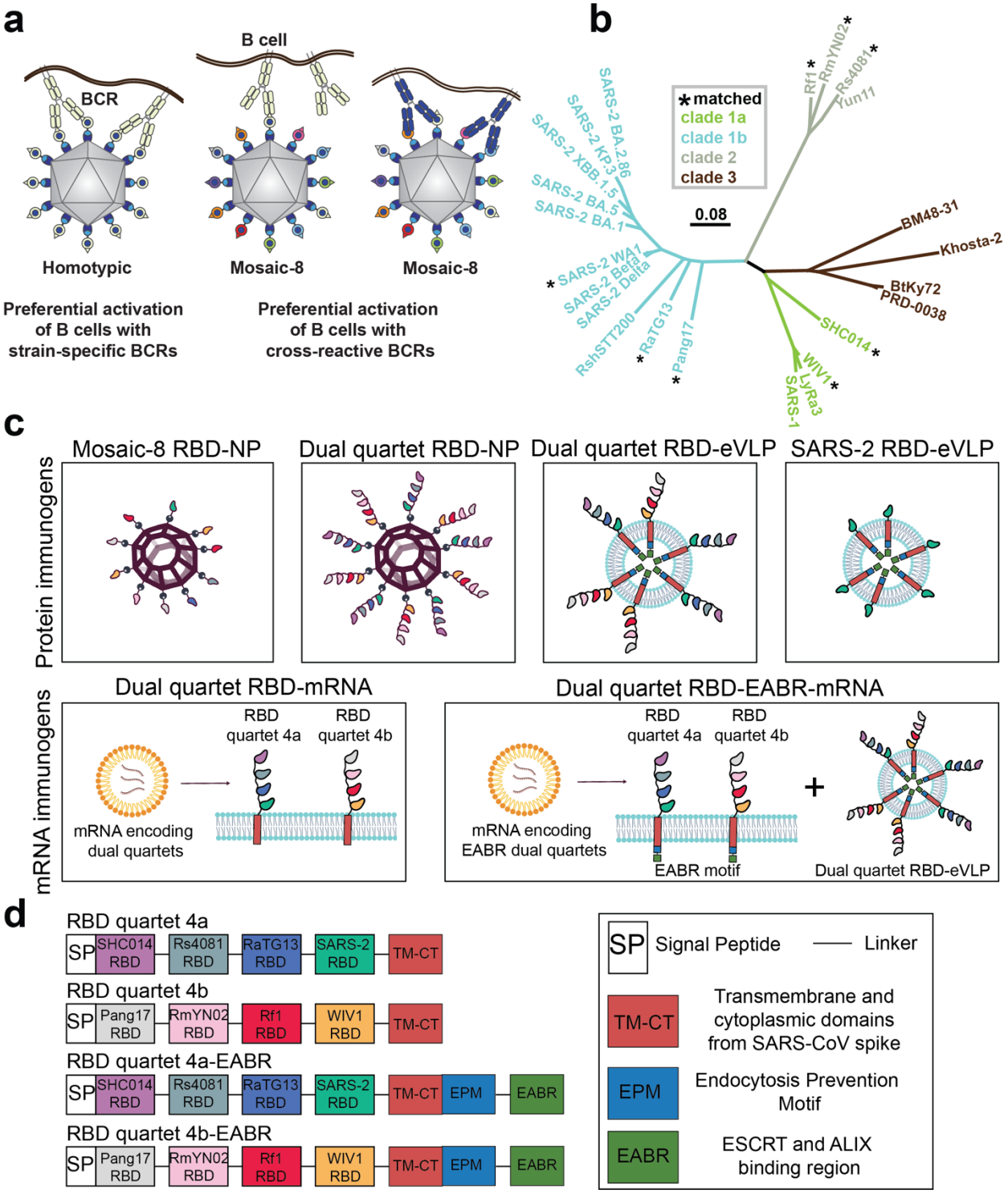

Figure 1. Protein- and mRNA-based pan-sarbecovirus immunogens.
(a) Avidity hypothesis. Left: Membrane-bound strain-specific BCRs (pale yellow) using avidity to recognize a strain-specific epitope (pale yellow triangle) on antigens attached to a homotypic NP. Middle: Strain-specific BCRs binding with only a single Fab (i.e., not using avidity) to a strain-specific epitope (triangle) on an antigen attached to a mosaic NP. Right: Cross-reactive BCRs using avidity to recognize a common epitope (blue circle) presented on different antigens attached to a mosaic NP, but not to strain-specific epitopes (triangles). Only a fraction of the 60 attached RBDs are shown for clarity. (b) Sarbecovirus phylogenetic tree (made using a Jukes-Cantor generic distance model with Geneious Prime® 2023.1.2) calculated from amino acid sequences of RBDs aligned using Clustal Omega[17]. Viruses with RBDs included in RBD quartets and mosaic-8 RBD-NPs are indicated with an asterisk. Scale bar = phylogenetic distance of 0.08 nucleotide substitutions per site. (c) Schematics of protein-based and mRNA-based pan-sarbecovirus immunogens (not to scale; showing only a fraction of antigens for clarity). (d) Schematics of mRNA constructs encoding RBD dual quartet immunogens used in this study.

Conversion of dual RBD quartet immunogens to an mRNA format (Fig. 1c; dual quartet RBD-mRNA) also offers the possibility of using the ESCRT- and ALIX-binding region (EABR) mRNA vaccine platform, which results in presentation of immunogens on cell surfaces and on circulating enveloped virus-like particles (eVLPs), thereby combining attributes of both mRNA and protein-NP vaccines[8] (Fig. 1c; dual quartet RBD-EABR-mRNA). eVLP formation is achieved by appending a short EABR sequence to the cytoplasmic domain of the mRNA-encoded immunogen, which recruits cellular ESCRT proteins to induce eVLP budding from the plasma membrane[8]. We previously showed that two immunizations with mRNA-LNP encoding spike-EABR elicited potent CD8+ T-cell responses and superior neutralizing antibody responses against original and variant SARS-2 compared to conventional spike-encoding mRNA-LNP and purified spike-EABR eVLPs, improving neutralizing titers >10-fold against Omicron-based variants.

Here, we show that the advantages of protein-based mosaic-8 RBD-NP vaccines can be transferred to an mRNA-LNP vaccine format. We compared immune responses in mice immunized with dual quartet RBD-mRNA versions of mosaic-8 immunogens (dual quartet RBD-mRNA and dual quartet RBD-EABR-mRNA) with responses to two versions of protein-based mosaic-8 NPs (dual quartet RBD-NP[7] and EABR-based dual quartet RBD-eVLPs) or to homotypic SARS-2 RBD-eVLPs. Immunization with mRNA immunogens elicited equivalent or improved binding breadths, neutralization potencies, T cell responses, and targeting of conserved RBD epitopes across sarbecoviruses compared to protein-based mosaic-8 immunogens, demonstrating successful conversion of the mosaic-8 RBD vaccine to mRNA formats that enable streamlined, scalable manufacturing of a pan-sarbecovirus vaccine.

Results

mRNA-encoded RBD quartets are presented on cell surfaces and eVLPs

mRNA-LNP can direct cell surface expression of a variety of gene products, including viral antigens[18]. We investigated whether protein-based soluble dual quartets could be modified to induce cell surface expression by creating constructs that encode an RBD quartet followed by a linker, transmembrane anchoring sequence, and cytoplasmic tail (Fig. 1d; RBD quartets 4a and 4b). The eight RBDs in the 4a and 4b quartet sequences correspond to the RBDs used in previous studies investigating dual quartet RBD-NPs constructed from soluble quartets[7] and to RBDs in a mosaic-8 RBD-NP constructed from soluble monomeric RBDs[2] (Fig. 1b). We used flow cytometry

to verify presentation of membrane-bound RBD quartets on the surface of cells transfected with mRNA encoding RBD quartet 4a or RBD quartet 4b by staining with C118, a human mAb that recognizes a conserved RBD epitope present on all eight RBDs[19,20]. Flow cytometry results showed high and equivalent levels of RBD quartets 4a and 4b on cell surfaces when each was expressed separately (Extended Data Fig. 1a).

We next investigated the use of EABR technology, which modifies membrane proteins delivered by mRNA-LNP to induce self-assembly and budding of eVLPs, resulting in immunogen presentation on cell surfaces and circulating eVLPs[8], for delivering quartet RBD sequences. eVLP assembly is induced by appending a short amino acid sequence to the cytoplasmic domain of a membrane protein, which recruits proteins from the host ESCRT pathway that drives budding for many enveloped viruses[21]. Addition of an EABR sequence has been shown to produce eVLPs for a variety of membrane proteins including SARS-2 spike[8], HIV-1 Env[8], influenza hemagglutinin[22], RSV fusion protein[8] (class I viral fusion protein trimers), Andes virus glycoprotein (a tetramer)[23], CCR5 (a G protein-coupled receptor with multiple transmembrane regions)[8], epidermal growth factor receptor[23], and MHC class I proteins[24]. Compared to non-EABR RBD quartets, cells expressing EABR-modified RBD quartets showed lower cell surface expression by flow cytometry using the pan-sarbecovirus RBD-specific C118 Ab[19,20] (Extended Data Fig. 1a). Lower cell surface expression for an EABR-containing membrane protein, which was also found when comparing SARS-2 spike trimer expression plus and minus an EABR sequence[8], is presumably due to incorporation of a subset of cell surface proteins into released eVLPs that are not retained on the cell surface.

To evaluate whether the RBD quartet 4a-EABR and 4b-EABR constructs induced secretion of RBD quartet-displaying eVLPs, we subjected supernatants of quartet 4a- or 4b–transfected cells to an established eVLP purification procedure[8]. ELISAs were consistent with efficient eVLP formation for EABR mRNAs, showing high quartet 4a or 4b protein levels in the purified eVLP samples for EABR, but not non-EABR, quartets (Extended Data Fig. 1b). We also used Abs specific for quartet 4a (anti-Rs4081 RBD)[25] and 4b (anti-WIV1 RBD)[26] to examine co-transfected cells by flow cytometry, demonstrating that RBD quartets 4a and 4b were co-expressed at the surface of individual cells (Extended Data Fig. 1c). To confirm that both quartets were incorporated into the same eVLP, we used a sandwich ELISA to probe eVLPs resulting from an RBD quartet 4a-EABR and 4b-EABR co-transfection. eVLPs were purified from co-transfected cells, captured with anti-WIV1 RBD Ab (quartet 4b), and detected with anti-Rs4081 RBD Ab (quartet 4a), verifying the presence of both quartets on dual quartet eVLPs (Extended Data Fig. 1d). As expected, no binding was detected for samples prepared in the same way from cells co-transfected with non-EABR versions of the quartets or cells only transfected with quartet 4a-EABR or 4b-EABR (Extended Data Fig. 1d). Taken together, these data show that mRNA-encoded RBD quartets were co-expressed on the surface of transfected cells and that the two EABR-modified quartets are co-displayed on eVLPs.

Dual quartet RBD mRNA immunogens elicit cross-reactive Abs

We next compared Ab responses in mice immunized with mRNA-encoded dual quartets to immunizations with protein-based dual quartet RBD-NPs or with purified dual quartet RBD-eVLPs. For mRNA immunizations, mRNA encoding RBD quartets 4a and 4b were co-formulated into lipid nanoparticles (LNP) to generate dual quartet immunogens (dual quartet RBD-mRNA and dual quartet RBD-EABR-mRNA), which were each injected intramuscularly at RNA doses of 1.5 µg or 0.5 µg (Fig. 2a, Extended Data Fig. 2a). We also included cohorts of mice that were immunized with 5 µg of dual quartet RBD-NPs (calculated based on RBD content) in the presence

of adjuvant (Fig. 2a) and cohorts immunized with adjuvanted purified RBD-eVLPs (dual quartet RBD-eVLP or SARS-2 RBD-eVLP; 5 μg RBD content per dose), the latter representing a homotypic immunogen control presenting only one type of RBD (Fig. 1c).

Because binding and neutralizing Ab responses both correlate with protection in humans and animals vaccinated with COVID-19 mRNA vaccines[27-29], we analyzed immunized mouse sera by ELISA to evaluate Ab binding responses and used pseudovirus assays[30] to evaluate neutralization (Fig. 2b,c; Extended Data Fig. 2b). When comparing mRNA-based to protein-based immunogens, we used a 1.5 μg mRNA dose and a 5 μg (RBD content) dose for the protein-based immunogens (Fig. 2b,c), which represent standard doses used for these vaccine modalities in mice[2,8,31]. We also compared the mRNA and mRNA-EABR immunogens using a 0.5 μg mRNA dose to investigate potential dose-sparing effects of the EABR technology (Extended Data Fig. 2b). To evaluate potential sarbecovirus strain-specific differences in Ab binding and neutralization properties, we displayed data to show responses to individual sarbecovirus antigens (Fig. 2b,c; left panels) and also as the overall geometric mean (geomean) response elicited by the different cohorts across evaluated antigens, a form that allows statistical evaluation of differences across different cohorts (Fig. 2b,c; right panels).

The highest mean binding titers for sera from the five cohorts across a panel of matched and mismatched sarbecovirus RBDs were found for dual quartet RBD-mRNA and dual quartet RBD-EABR-mRNA (Fig. 2b, left). Thus, genetically encoded RBD quartets delivered by a 1.5 μg dose of mRNA-LNPs were significantly more effective at eliciting cross-reactive RBD-binding Abs across a panel of sarbecovirus RBDs than 5 μg of the dual quartet RBD-NP protein-based immunogen (Fig. 2b, right; $p<0.0001$ for comparisons of dual quartet RBD-mRNA and dual quartet RBD-EABR-mRNA). In addition, both dual quartet RBD-mRNA and dual quartet RBD-EABR-mRNA exhibited significantly higher geomean binding titers than the protein-based dual quartet RBD-eVLPs and homotypic SARS-2 RBD-eVLPs (Fig. 2b, right; $p<0.0001$ for all comparisons of mRNA-LNP immunogens and protein-based immunogens). SARS-2 RBD-eVLPs exhibited significantly lower binding titers across the RBD panel than the dual quartet RBD-NPs and purified dual quartet RBD-eVLPs (Fig. 2b, right; $p<0.0001$ for all comparisons except comparing with dual quartet RBD-eVLP, where $p=0.0057$), as expected based on results for homotypic RBD-NPs[2,3].

We also compared neutralizing titers elicited by the five cohorts across a panel of matched and mismatched sarbecovirus strains (Fig. 2c, left). When comparing neutralization titers by strain between the five immunization cohorts, dual quartet RBD-mRNA, dual quartet RBD-EABR-mRNA, and dual quartet RBD-NP exhibited the highest titers across the pseudovirus panel except for neutralization of SARS-2 D614G, where homotypic SARS-2 RBD-eVLPs showed induction of slightly higher titers (Fig. 2c, left). Geomean neutralization titers for the five cohorts (Fig. 2c, right) were more similar to each other than the mean binding titers (Fig. 2b, right) but dual quartet RBD-EABR-mRNA induced significantly higher mean neutralizing titers than dual quartet RBD-NP ($p=0.0152$), dual quartet RBD-eVLP ($p=0.0152$), and SARS-2 RBD-eVLP ($p=0.0470$).

To investigate the effects of lower doses of the mRNA immunogens, we measured binding and neutralization titers elicited by 0.5 μg doses of dual quartet RBD-mRNA and dual quartet RBD-EABR-mRNA immunizations (Extended Data Fig. 2a,b). Binding titers against the RBDs tested were not statistically different for the two mRNA immunogens, except for binding to the BM48-31 RBD, in which case the dual quartet RBD-EABR-mRNA immunization induced significantly higher binding than the dual quartet RBD-mRNA immunization (Extended Data Fig. 2b, left;

p=0.0089). Neutralization titers were significantly different for three viruses: SARS-2 D614G, where titers were higher for dual quartet RBD-mRNA (p=0.00013), and for SARS-1 (p=0.00024) and WIV1 (p<0.0001), where titers were higher for dual quartet RBD-EABR-mRNA (Extended Data Fig. 2b, right panel). These results are consistent with the more potent neutralization of non-SARS-2 viruses induced by dual quartet RBD-EABR-mRNA compared with dual quartet RBD-mRNA at the 1.5 μg dose (Fig. 2c).

Despite eliciting high binding titers against both SARS-2 variants and non-SARS-2 sarbecoviruses, neutralization titers for mosaic-8 immunogens (dual quartet RBD mRNAs, dual quartet RBD-NP, and dual quartet RBD-eVLP) were lower against SARS-2 variants than against non-SARS-2 sarbecoviruses (Fig. 2c, Extended Data Fig. 2b). Importantly, however, binding Abs can trigger immune responses to clear infected cells through Fc-mediated effector functions[32] and/or complement activation[33]. Indeed, human mAbs that neutralized early SARS-2 strains but lost neutralizing activity against SARS-2 Omicron variants retained Fc effector functions[32], and non-neutralizing human anti-RBD mAbs protected from a SARS-2 challenge in animal models[34]. Thus, even in the absence of strong neutralizing titers against SARS-2 variants, the ability of mosaic-8 immunogens to elicit Abs that exhibit broad binding across sarbecovirus RBDs is a desirable trait for a protective pan-sarbecovirus vaccine.

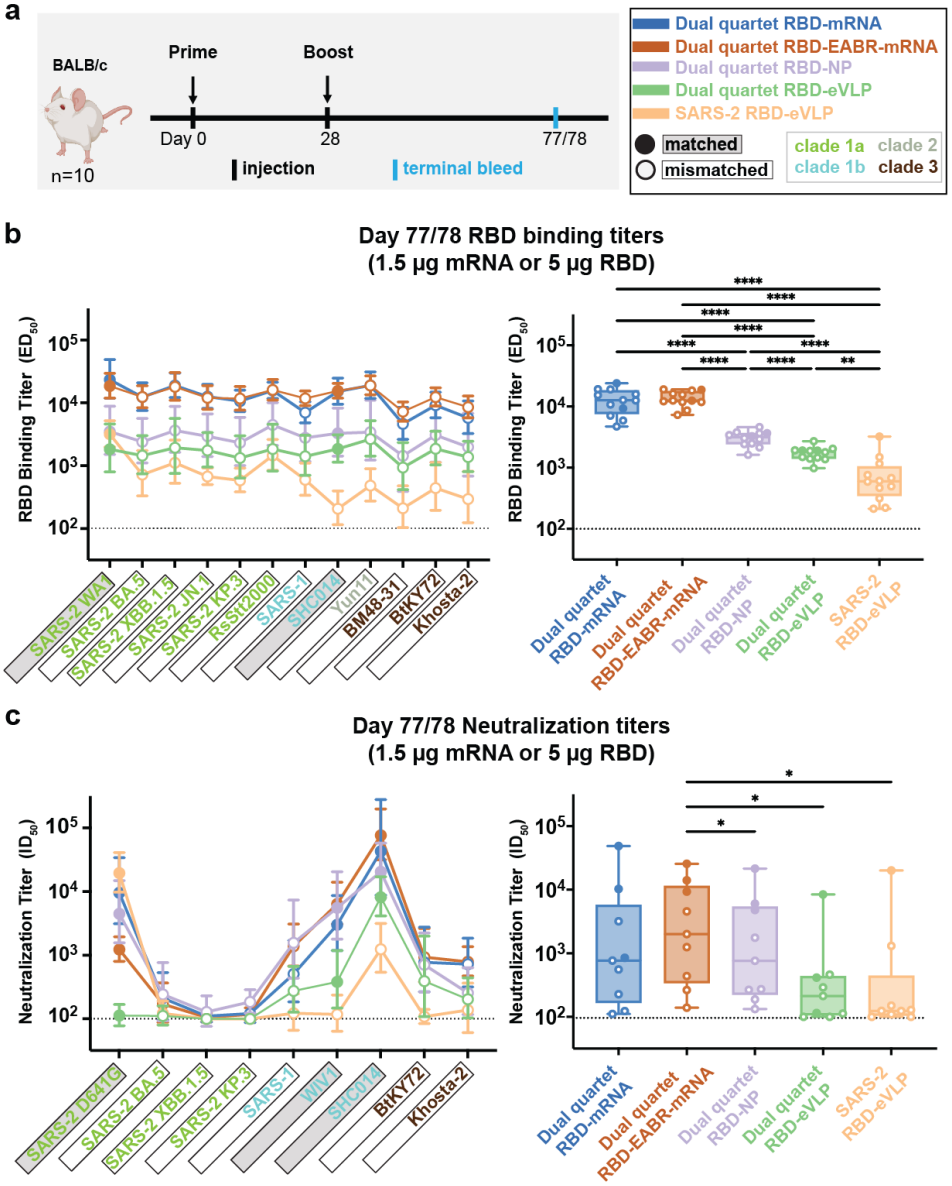

Figure 2. Dual quartet RBD mRNA immunogens elicit cross-reactive Abs.
ELISA and neutralization results for terminal bleed serum samples (see also Extended Data Fig. 2). (a) Immunization regimen. Left: Mice were primed at day 0, boosted at day 28, and samples were collected from a terminal bleed at day 77 or 78. Right: Colors used to identify immunization cohorts and symbols indicating a sarbecovirus antigen or pseudovirus that is matched (filled in data points; gray shading around name) or mismatched (unfilled data points; black outline around name). Sarbecovirus strain names are colored in panels b and c according to clade. (b,c) Results for RBD-binding ELISAs (panel b) and pseudovirus neutralization assays (panel c) for serum samples from day 77 or 78. Dashed horizontal lines indicate detection limits for assays. Left: Geomeans of RBD-binding ELISA half-maximal effective dilution (ED_{50}) values (panel b) or neutralization half-maximal inhibitory dilution (ID_{50}) values (panel c) across a panel of viral antigens or pseudoviruses for sera from animals in each cohort (geomeans are plotted as symbols with geometric standard deviations indicated by error bars). Mean ED_{50} or ID_{50} values across antigens are connected by colored lines corresponding to the immunization cohort. Right: Box and whisker plots of geomean responses (ELISA ED_{50}s in panel b; neutralization ID_{50}s in panel c) with individual data points representing geomean responses across n=10 sera to a single antigen or

pseudovirus. Geomean titers were compared pairwise between immunization cohorts by Tukey's multiple comparison test with the Geisser-Greenhouse correction (as calculated by GraphPad Prism). Significant differences between cohorts are indicated by asterisks: $p<0.05$ = *, $p<0.01$ = **, $p<0.001$ = ***, $p<0.0001$ = ****.

mRNA-encoded dual quartets elicit potent T cell responses

T cell responses to the various immunogens were evaluated on day 77/78 in splenocytes from immunized mice using enzyme-linked immunosorbent spot (ELISpot) assays[35]. Secretion of IFN-γ (a cytokine produced by CD4+ T helper 1 (T_H1) cells and cytotoxic CD8+ T cells) and IL-4 (a cytokine produced by CD4+ T helper 2 (T_H2) and T follicular helper cells[36]) was measured after splenocytes were stimulated with a pool of SARS-2 spike peptides.

The dual quartet RBD-mRNA and dual quartet RBD-EABR-mRNA cohorts exhibited potent IFN-γ responses, consistent with activation of RBD-specific cytotoxic CD8+ T cells, whereas low/undetectable IFN-γ responses were found for the protein-based dual quartet RBD-NP, dual quartet RBD-eVLP, and SARS-2 RBD-eVLP cohorts, results consistent with previous findings for mice immunized with purified spike-EABR eVLPs[8] and the fact that mRNA-LNP immunogens, but not protein immunogens, promote intracellular expression of antigens that serve as sources for peptides loaded onto MHC class I proteins[37]. We found strong IL-4 responses for both the mRNA and protein-based immunogen cohorts (Fig. 3).

Thus, mRNA-based mosaic-8 dual RBD quartet immunizations induce superior (INF-γ) or equivalent (IL-4) release of cytokines compared with protein-based mosaic-8 immunogens.

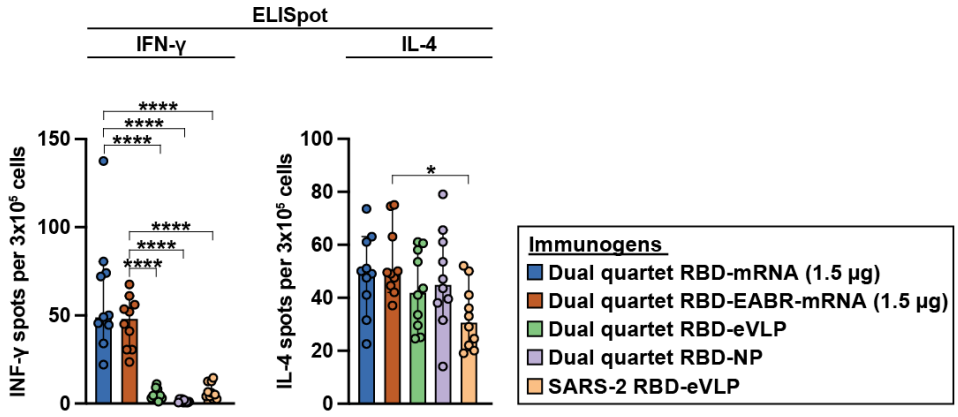

Figure 3. mRNA-encoded dual quartets elicit potent T cell responses. ELISpot assay data for SARS-2 RBD-specific IFN-γ (left) and IL-4 (right) responses of splenocytes from BALB/c mice that were immunized with the indicated immunogens (immunization regimen in Fig. 2a). Results are shown as spots per $3x10^5$ cells for individual mice (colored circles) presented as the median (bars) and standard deviation (horizontal lines). Cohorts were compared by Tukey's multiple comparison test calculated by GraphPad Prism. Significant differences between cohorts linked by horizontal lines are indicated by asterisks: $p<0.05$ = *, $p<0.0001$ = ****.

mRNA-encoded and protein-based dual quartets elicit Abs targeting similar epitopes

To investigate which RBD epitopes were targeted by Abs elicited by the different vaccine modalities, we used DMS to evaluate the effects of all possible amino acid changes in an RBD on binding to polyclonal serum Abs[15,38-43]. To interpret results, we classified RBD residues by

epitopes that were defined based on structural properties and conservation/variability across sarbecoviruses: class 1 and class 2 RBD epitopes exhibit more sequence variability across sarbecoviruses and SARS-2 variants, and class 4, class 1/4, and portions of class 3 and class 5 epitopes are more conserved[20,44-46] (Fig. 4a). In some DMS analyses of polyclonal serum Abs, we observed weak escape profiles that lacked clear features, which we defined as a "polyclass," i.e., a more balanced, response[4]. We interpreted polyclass responses as resulting from sera containing multiple classes of anti-RBD Abs based on control experiments in which we evaluated equimolar mixtures of anti-RBD monoclonal Abs that targeted multiple epitopes[4]. For the current experiments, we analyzed serum using yeast display libraries encoding RBDs derived from SARS-2 WA1 (matched) and SARS-1 (mismatched) spike proteins.

DMS results showed that the epitopes targeted in both RBD libraries by the mRNA-encoded dual quartet RBD immunogens were similar overall to each other and to epitopes targeted by the protein-based dual quartet RBD-NP immunogen (Fig. 4b,c; Table 1, Extended Data Figs. 3, 4). In particular, the dual quartet immunogens, like mosaic-8 RBD-NPs[3,4], did not primarily elicit Abs against the immunodominant and variable class 1 and class 2 RBD epitopes, as observed for Abs elicited by homotypic SARS-2 RBD NPs[3,4] and spike-based mRNA vaccines[47]. Instead, elicited Abs primarily targeted class 4 and class 5 RBD epitopes, except for the Abs raised by immunization with dual quartet RBD-NPs, where class 5 was the predominant targeted epitope.

Although dual quartet RBD immunizations resulted in a mixed class 4/class 5 RBD response when evaluated against the SARS-2 WA1 and SARS-1 RBD libraries (Fig. 4b,c; Table 1, Extended Data Figs. 3, 4), there were notable differences. For example, both RNA-based immunogens elicited similar class 4 and class 5 RBD responses, but dual quartet RBD-mRNA sera showed more of a class 1/class 2 RBD response than dual quartet RBD-EABR-mRNA sera against the SARS-2 WA1 RBD library (Fig. 4b; Table 1), perhaps explaining why dual quartet RBD-mRNA elicited higher neutralization titers against the matched SARS-2 D614G pseudovirus (Fig. 2c, Extended Data Fig. 2b). Against the SARS-1 RBD library, each of the dual quartet immunogens induced strong class 4 and class 5 responses. In addition, weak escape by Abs against the variable class 1 and class 2 RBD epitopes was seen for dual quartet RBD-mRNA, dual quartet RBD-EABR-mRNA, and dual quartet RBD-NP (Table 1). Finally, one mouse in the dual quartet RBD-EABR-mRNA group and two in the dual quartet RBD-NP group elicited polyclass responses, consistent with the ability of these dual quartet immunogens to induce Abs against multiple RBD epitopes.

We conclude that converting dual quartet RBD immunogens into an mRNA format retains the ability of mosaic-8 vaccines to elicit Abs mainly against more conserved RBD regions, as previously observed in DMS experiments comparing protein NPs presenting dual RBD quartets or eight monomeric RBDs[7].

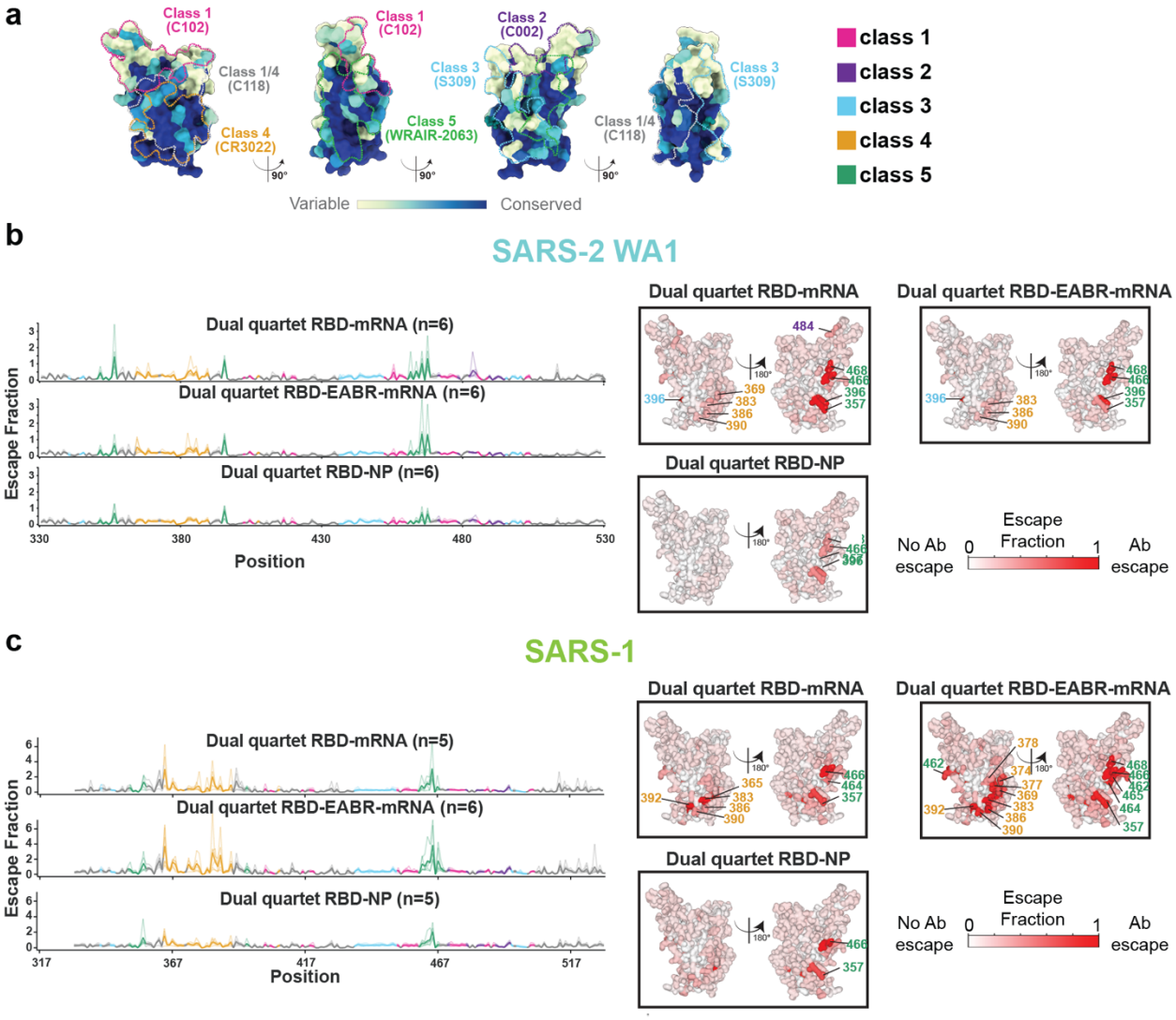

Figure 4. Dual quartet RBD-mRNA immunogens elicit Ab responses against conserved class 4 and class 5 RBD epitopes.

(a) Sequence conservation of 16 sarbecovirus RBDs calculated using ConSurf[48] shown on a surface representation of SARS-2 RBD (PDB 7BZ5). Class 1, 2, 3, 4, 1/4, and 5 anti-RBD Ab epitopes[20,44-46] are outlined in dots in different colors using information from representative structures of Abs bound to SARS-2 spike or RBD (C102: PDB 7K8M; C002: PDB 7K8T, S309: PDB 7JX3; CR3022: PDB 7LOP; C118: PDB 7RKV; WRAIR-2063: PDB 8EOO). (b,c) Left: Line plots for DMS results using a SARS-2 WA1 RBD library (b) and SARS-1 library (c) from the indicated number of mice immunized with the immunogens listed above each line plot. X-axis: RBD residue number. Y-axis: sum of the Ab escape of all mutations at a site (larger numbers = more Ab escape). Each line represents one antiserum with thick lines showing the average across the n = 5 or 6 sera in each group. Lines are colored according to RBD epitopes in panel a. Right: Average site-total Ab escape calculated for results from n = 5 or 6 serum samples for the indicated RBD yeast display libraries. Mice were immunized with the immunogens listed, and results were

mapped to the highlighted residues on the surface of the SARS-2 WA1 RBD (PDB 6M0J). Gray indicates no escape; a gradient of red represents increasing degree of escape. Residue numbers show sites with the most escape with font colors representing different RBD epitopes (defined in panel a; class 1/4 residues are colored with fonts corresponding to class 1 or class 4 residues). The same data are shown in Table 1 and in Extended Data Figs. 3 and 4 (line and logo plots for SARS-2 WA1 and SARS-1 RBD libraries, respectively).

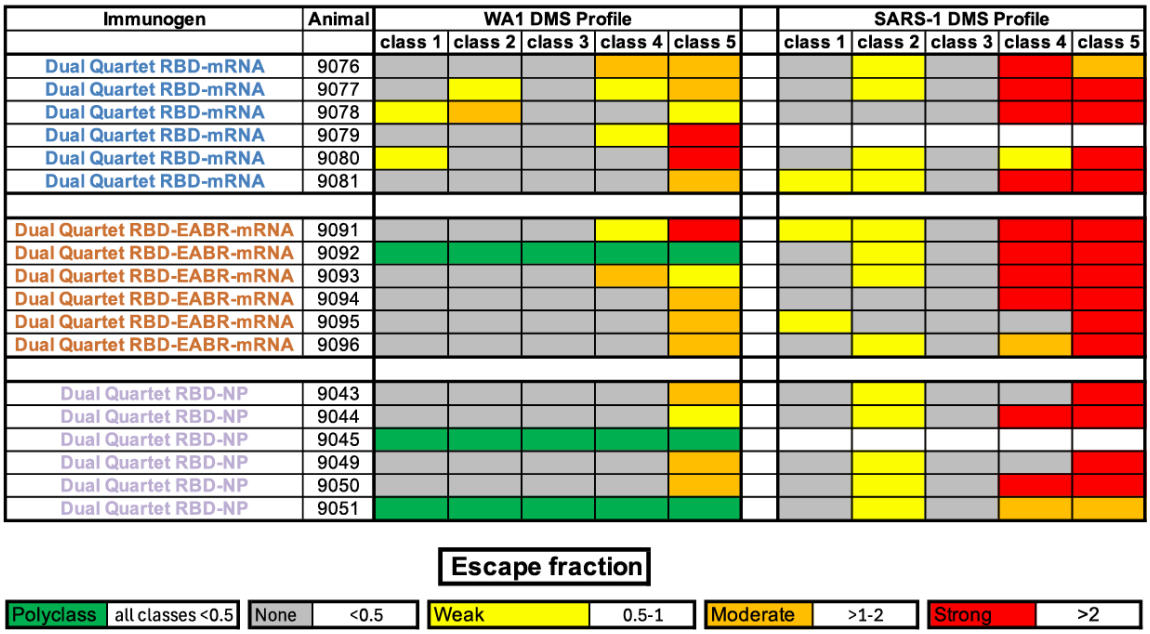

Table 1. Summary of DMS data showing elicitation of strong Ab responses against class 4 and class 5 RBD epitopes by dual quartet RBD-mRNA immunogens.
Results for individual mice are shown with ID numbers indicated. DMS was conducted using a SARS-2 WA1 RBD library (left) or a SARS-1 RBD library (right). DMS profiles were classified as polyclass, weak, moderate, or strong as indicated by the maximum escape fraction for any RBD position in each RBD epitope class. Colors and different designations for epitopes were assigned as indicated at the bottom (white entries for animals 9079 and 9045 indicate that no data were available). See also Fig. 4 and Extended Data Figs. 3, 4.

mRNA-encoded dual quartet RBD immunogens elicit balanced IgG2a/IgG1 responses

IgG subclasses induce distinct Fc effector functions, including opsonization, phagocytosis, and Ab-dependent cell-mediated cytotoxicity, through differential binding of their Fc domains to Fc gamma receptors (FcγRs)[49]; e.g., mouse IgG1, IgG2a, and IgG2b bind the activating receptor FcγR3 and the inhibitory receptor FcγR2b, IgG2a and IgG2b bind the activating receptor FcγR4, and mouse IgG3 does not bind detectably to any of these FcγRs[50]. Of the activating receptors, FcγR3 is more widely expressed than FcγR4, with FcγR4 mainly expressed on monocytes/macrophages and neutrophils and FcγR3 found on those cells plus dendritic cells, natural killer cells, basophils, mast cells, and eosinophils[50]. In immunized mice, IgG2a is associated with T_H1-type immune responses, effective activation of complement, and protective interactions with FcγRs, which are critical functions for clearing viruses[51]. IgG1, although usually efficient in neutralization of viruses, is associated with T_H2-type responses, which are thought to be less effective than T_H1 responses in anti-viral immune defense[52].

We used systems serology[9] to evaluate the IgG distributions elicited by mRNA versus protein immunogens by comparing binding of IgG1, IgG2a, IgG2b, IgG3, FcγR2b-, FcγR3-, or FcγR4-binding IgGs, and total IgG (defined as IgGs isolated using a pan-IgG Ab) elicited by the five immunogens to a panel of spike trimers and RBDs derived from SARS-2 variants and other sarbecoviruses. Results are presented to show the elicited responses from individual mice to each antigen (Fig. 5) and geomean responses across the antigens for each immunogen (Extended Data Fig. 5).

Both dual quartet RBD-mRNA immunogens elicited high levels of IgG1 and IgG2a against a broad panel of sarbecovirus spikes and RBDs, with somewhat higher levels of IgG2a than IgG1 (Fig. 5, Extended Data Fig. 5), demonstrating a desirable mixture of IgGs for an anti-viral vaccine of induced T_H1 and T_H2 responses. In addition, the mRNA-based immunogens each elicited significantly higher IgG2a and FcγR4-binding IgG responses than the protein-based immunogens ($p<0.0001$) (Extended Data Fig. 5). The protein-based dual quartet RBD-NP and dual quartet RBD-eVLP immunogens elicited higher levels of IgG1 than IgG2a, consistent with their administration with Addavax adjuvant, which enhances T_H2-biased immune responses[53]. Dual quartet RBD-eVLPs also elicited significantly higher IgG2a responses than dual quartet RBD-NPs ($p<0.0001$). Interestingly, dual quartet RBD-EABR-mRNA elicited significantly higher IgG2b ($p<0.0001$), as well as FcγR3- ($p=0.0013$) and FcγR4- ($p=0.0021$) binding IgGs, than dual quartet RBD-mRNA. Finally, consistent with earlier demonstrations of the more limited sarbecovirus recognition properties of Abs raised in response to homotypic RBD-NPs[2-4,25], the SARS-2 RBD-eVLP immunogen elicited IgGs mainly against SARS-2 and closely related RBDs (Fig. 5).

Taken together, these results demonstrate that the mRNA versions of dual quartet immunogens elicit balanced IgG responses that recognize a broad range of sarbecovirus antigens, arguing for their likely efficacy to protect against diverse sarbecoviruses.

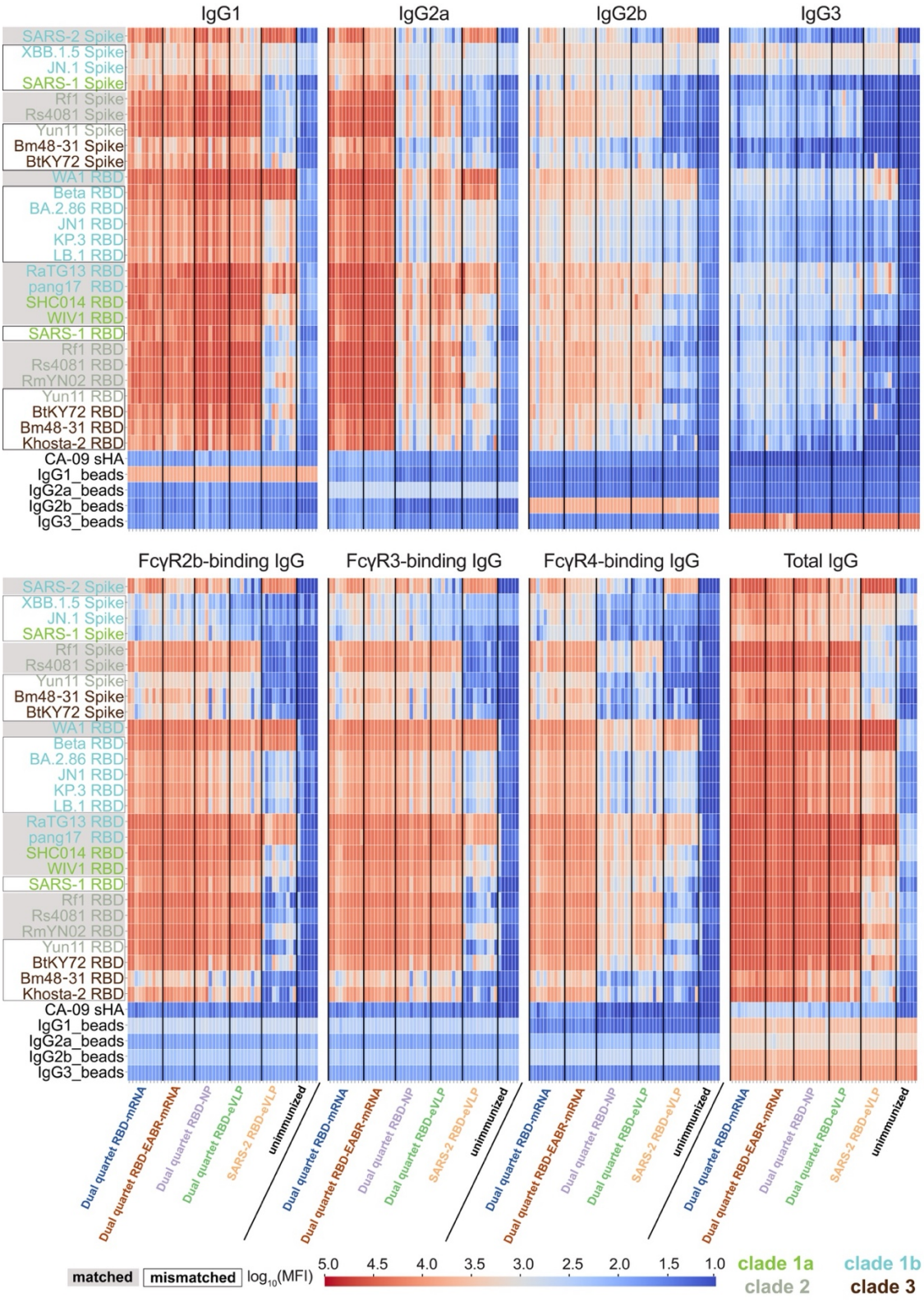

Figure 5. mRNA-encoded dual quartet RBD immunogens elicit balanced IgG subclass and potent FcγR-binding responses.

MFI = median fluorescent intensity. Binding of IgG1, IgG2a, IgG2b, IgG3, FcγR2b-binding IgGs, FcγR3-binding IgGs, FcγR4-binding IgGs, and total IgG to the indicated spikes, RBDs, or non-

sarbecovirus control proteins. Antigen names (y-axes) are colored according to spike or RBD clades. Matched antigens are indicated with gray shading around the name, and mismatched antigens are indicated with a black outline around the name. Each column represents binding data from an individual mouse, and immunization cohorts are separated by a vertical black line. A soluble influenza hemagglutinin trimer (CA-09 sHA) was used as a control to evaluate non-specific binding. See also Extended Data Fig. 5.

Systems Serology-Polyclonal Epitope Mapping (SySPEM)

To further explore potential differences in RBD recognition properties by different IgG subclasses within polyclonal Ab samples, we combined systems serology with epitope mapping in a new methodology we call Systems Serology-Polyclonal Epitope Mapping (SySPEM) (Extended Data Fig. 6), by analogy to Electron Microscopy-based Polyclonal Epitope Mapping[54] (EMPEM). For the epitope mapping aspect of SySPEM, we created epitope knock-out (KO) mutants in the SARS-2 WA1 RBD by introducing one or more potential N-linked glycosylation sites (PNGSs) to direct addition of N-glycan(s) in RBD epitopes that are recognized by either class 1 and class 2, class 2 only, class 3, class 1/4, class 4, or class 5 anti-RBD mAbs (Extended Data Fig. 7a). Addition of N-glycan(s) at the introduced PNGS(s) was verified by SDS-PAGE of purified RBD KO proteins, and correct folding and epitope blocking were verified by ELISA using a panel of control mAbs (Extended Data Fig. 7b,c). We measured binding of total polyclonal IgG and IgG subsets to unmodified (wildtype; wt) WA1 RBD and to each of RBD KO mutants, defining a SySPEM score for each IgG sample/epitope pair as [1.0 – (RBD KO binding / RBD wt binding) x 100]; thus, higher SySPEM scores indicate increased binding by a particular IgG class to that epitope (Extended Data Fig. 6). We present SySPEM results in three formats to visualize epitope recognition across immunogens and antibody subclasses: (*i*) Median SySPEM scores from individual mice divided into distinct RBD epitopes recognized by different IgG classes with statistical comparisons between immunogen cohorts (Fig. 6). This comparison highlights differences in epitope recognition across immunogen cohorts. (*ii*) Median SySPEM scores for each IgG class within a given immunogen cohort with statistical comparisons between targeted epitopes (Extended Data Fig. 8). This shows the epitope distribution for a given immunogen/IgG class pair, allowing for epitope profile comparisons between different immunogens, analogous to a DMS profile (e.g., Fig. 4). (*iii*) Uniform Manifold Approximation and Projection (UMAP)[55] format to reduce the dimensions of the data set (Fig. 7). These figures provide hierarchical views of the SySPEM data: statistical comparisons across immunogens (Fig. 6), detailed within-cohort analyses (Extended Data Fig. 8), and global similarity mapping of antibody recognition patterns (Fig. 7).

SySPEM scores validated the epitope mapping approach using RBD KO mutants by showing significantly higher scores for total IgGs elicited by homotypic SARS-2 RBD-eVLPs than by other immunogens against variable epitopes (class 1/class 2, class 2) and little to no targeting of more conserved epitopes (class 4, class 1/4, class 5) (Fig. 6), as previously observed by DMS for homotypic SARS-2 RBD-NPs[3].

For IgG1, the mRNA- and protein-based dual quartet immunogens showed the highest class 5 SySPEM scores, with only dual quartet RBD-mRNA exhibiting a score that was not significantly higher than that of homotypic SARS-2 RBD-eVLPs (Fig. 6). In addition, dual quartet RBD-eVLPs and dual quartet RBD-EABR-mRNA exhibited class 4 and class 1/4 IgG1 SySPEM scores that were significantly higher than respective scores for SARS-2 RBD-eVLPs. Similarly, for IgG2a, the dual quartet immunogens all elicited significantly higher class 5 responses than homotypic SARS-2 RBD-eVLP, with both dual quartet RBD-EABR-mRNA and dual quartet RBD-eVLP featuring the highest class 5 SySPEM scores. Dual quartet RBD-EABR-mRNA, dual quartet RBD-

NP, and dual quartet RBD-eVLP also elicited higher class 4 SySPEM scores than SARS-2 RBD-eVLP. Interestingly, although not significant, dual quartet RBD-mRNA elicited a higher class 1/class 2 SySPEM score than dual quartet RBD-EABR-mRNA, and the opposite trend was observed for class 5. These differences might explain the more potent SARS-2 D614G neutralization elicited by dual quartet RBD-mRNA compared to dual quartet RBD-EABR-mRNA (Fig. 2c), since class 1 and class 2 anti-RBD Abs are potent against SARS-2 WA1[44]. However, the combination of higher class 5 and lower class 1/class 2 responses elicited by the dual quartet RBD-EABR-mRNA immunogen represents a more favorable epitope targeting profile for broad pan-sarbecovirus vaccine efforts. For IgG2b and IgG3, SySPEM scores were more similar across the different RBD epitope categories, although dual quartet RBD-eVLP showed significantly higher class 4 and class 5 SySPEM scores than SARS-2 RBD-eVLP.

For total IgG, dual quartet RBD-EABR-mRNA and dual quartet RBD-NP showed higher class 5 SySPEM scores than SARS-2 RBD-eVLP, with dual quartet RBD-eVLP showing the highest scores, and dual quartet RBD-mRNA showing class 5 scores that were not significantly higher than those exhibited by SARS-2 RBD-eVLP (Fig. 6). Dual quartet RBD-EABR-mRNA exhibited significantly higher class 4 and class 5 SySPEM scores for total IgG than dual quartet RBD-mRNA, likely driven by the stronger class 4 and class 5 targeting by IgG2a for this comparison (Fig. 6). Class 4 responses were higher for dual quartet RBD-EABR-mRNA, dual quartet RBD-NP, and dual quartet RBD-eVLP all exhibiting significantly higher class 4 SySPEM scores than SARS-2 RBD-eVLP, with dual quartet RBD-eVLP showing the highest class 4, 1/4, and 5 scores.

FcγR2b- and FcγR3-binding IgG SySPEM scores were similar across the RBD epitopes, with dual quartet RBD-EABR-mRNA, dual quartet RBD-NP, and dual quartet RBD-eVLP all exhibiting significantly higher class 5 SySPEM scores than SARS-2 RBD-eVLP (Fig. 6). Dual quartet RBD-eVLP and, to a lesser extent, dual quartet RBD-EABR-mRNA exhibited higher class 4 SySPEM scores than SARS-2 RBD-eVLPs. For FcγR4-binding IgGs, dual quartet RBD-EABR-mRNA, dual quartet RBD-NP, and dual quartet RBD-eVLP showed significantly higher class 4 and class 5 SySPEM scores than SARS-2 RBD-eVLP.

To identify all epitopes recognized by sera elicited by a given immunogen, we displayed the SySPEM results in a format in which SySPEM scores for recognition of individual RBD epitopes by different IgG classes are shown (Extended Data Fig. 8). These results highlight increased targeting of class 5 RBD epitopes by IgG1, IgG2a, IgG2b, and IgG3 subclasses elicited by the four dual quartet immunogens, but not by homotypic SARS-2 RBD-eVLPs. Interestingly, displaying the data in this format showed that in some cases for a given immunogen, different IgG subclasses can exhibit distinct epitope profiles, e.g., IgG1 and IgG2a from dual quartet EABR-mRNA cohort sera, where IgG1 showed higher class 1 and class 2 targeting than IgG2a, for which only class 5 targeting was high.

In order to visualize global patterns of epitope recognition between the different immunogens, we made UMAP plots[55] to project epitope profiles into two- or three-dimensional plots (Fig. 7). For 2D UMAP plots (Fig. 7a-e), clusters of points indicate samples that behaved similarly across all epitope knockouts, with ellipses indicating the spread of responses from each immunogen, and centroid markers (indicated by an X) indicating the average epitope mapping profile for each immunogen. When comparing IgG1 (Fig. 7a), IgG2a (Fig. 7b), IgG1, IgG2a, IgG2b, and IgG3 (Fig. 7c), and total IgG (Fig. 7d), epitope profiles for different immunogens showed similar trends with SARS-2 RBD-eVLP clustering farthest from the four dual quartet immunogens, and the dual

quartet immunogens showing more overlap with each other. Interestingly, dual quartet RBD-mRNA mapped closer to SARS-2 RBD-eVLP in all cases (Fig. 7a-e), as is especially apparent for IgG2a (Fig. 7b), total IgG (Fig. 7d), and the FcγRs (Fig. 7e). By contrast, dual quartet RBD-EABR-mRNA clustered further away from SARS-2 RBD-eVLP and closer to dual quartet RBD-eVLP. Dual quartet RBD-NP mapped similarly to dual quartet RBD-EABR-mRNA. To further assess differences in epitope recognition between different immunogens, a three-dimensional UMAP plot was generated using all data (Fig. 7f). Trends in the 3D map were consistent with the 2D UMAPs in that responses to the dual quartet immunogens were distinct from responses to SARS-2 RBD-eVLP and responses to dual quartet RBD-EABR-mRNA tended to map between dual quartet RBD-mRNA and the protein-based dual quartets, consistent with the EABR vaccine modality that combines traditional mRNA- and protein-based vaccinations[8]. In addition, the finding that SySPEM scores for dual quartet RBD-mRNA overlapped more with scores for SARS-2 RBD-eVLP than scores for the other dual quartet immunogens is consistent with more class 1/class 2 RBD epitope targeting by dual quartet RBD-mRNA and SARS-2 RBD-eVLP (Table 1).

Overall, the SySPEM studies confirmed targeting of more conserved RBD epitopes by the mRNA-based dual quartet immunogens, particularly the EABR-modified version, indicating successful conversion of the desirable properties of protein-based mosaic-8 immunogens. With detailed analyses, however, we found distinct epitope profiles for IgG subclass and FcγR-binding IgGs: i.e., the same antigens presented via different modalities (mRNA plus and minus EABR sequences and protein antigens on NPs or eVLPs) showed divergent SySPEM epitope profiles. In addition, SySPEM profiling of binding data can rationalize differences in neutralization profiles when comparing two similar immunogens presented differently (e.g., dual quartet RBD-EABR-mRNA versus dual quartet RBD-mRNA).

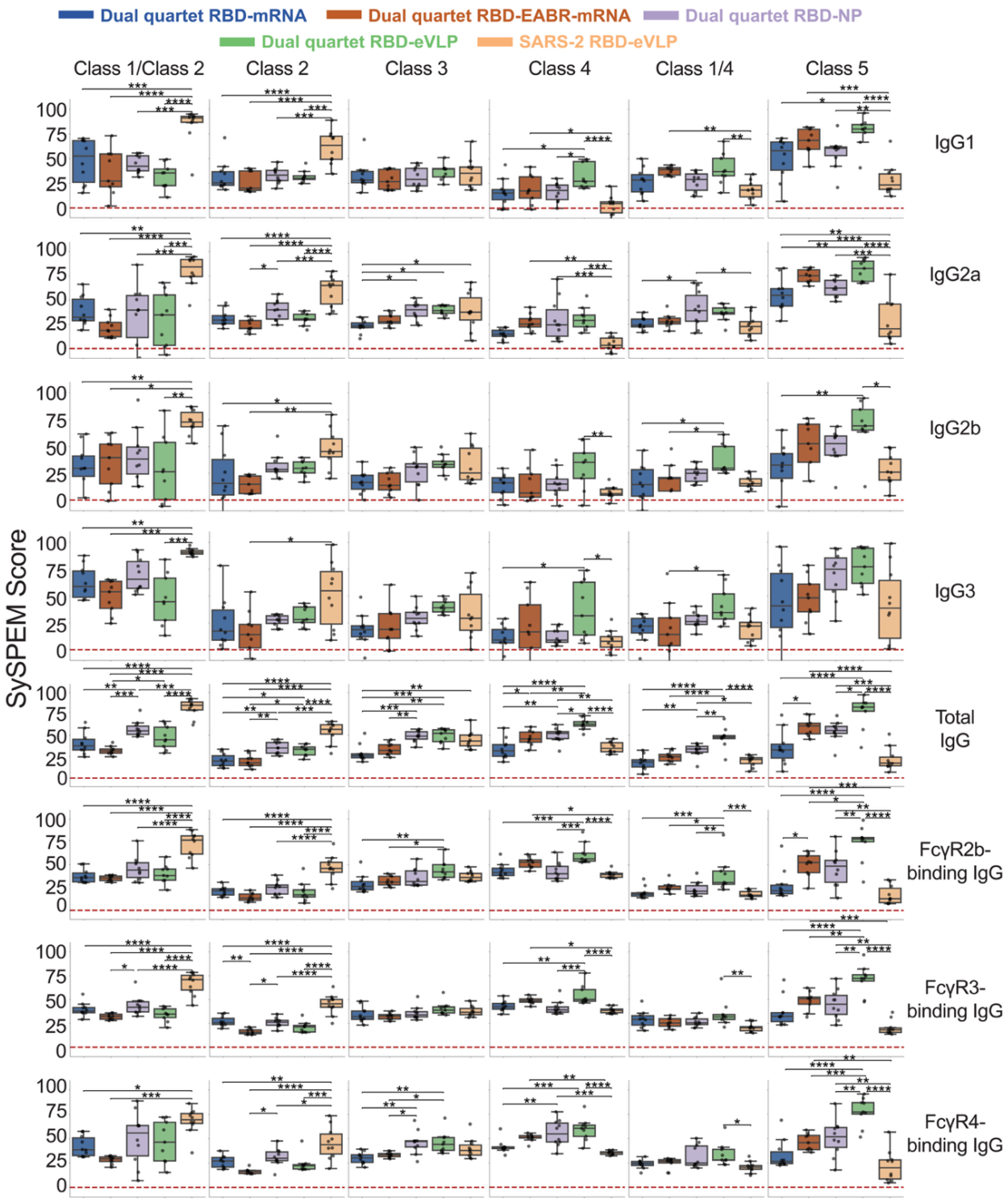

Figure 6. SySPEM score comparisons show differences in epitope recognition across immunogen cohorts.

SySPEM scores from individual mice were determined for RBD epitopes (columns) recognized by different IgG classes (rows, IgG subclass plus different FcγR-binding IgGs) with statistical comparisons between immunogen cohorts (colors). A SySPEM value of 0 indicates that none of the IgGs in that sample were affected by the glycan addition and therefore the sample did not contain IgGs that recognize that epitope, and a SySPEM value of 100 indicates that all IgGs in that

sample recognized that epitope (Extended Data Fig. 6). A SySPEM value between 0 and 100 indicates the proportion of IgGs in a sample that recognized the epitope that was blocked by glycan addition in the RBD KO mutant. Box and whisker plots of SySPEM scores with individual data points representing one mouse are shown. Significant differences between cohorts were calculated using Tukey's HSD posthoc test and linked by vertical lines indicated by asterisks: $p<0.05$ = *, $p<0.01$ = **, $p<0.001$ = ***, $p<0.0001$ = ****. See also Extended Data Fig. 8 and Fig. 7.

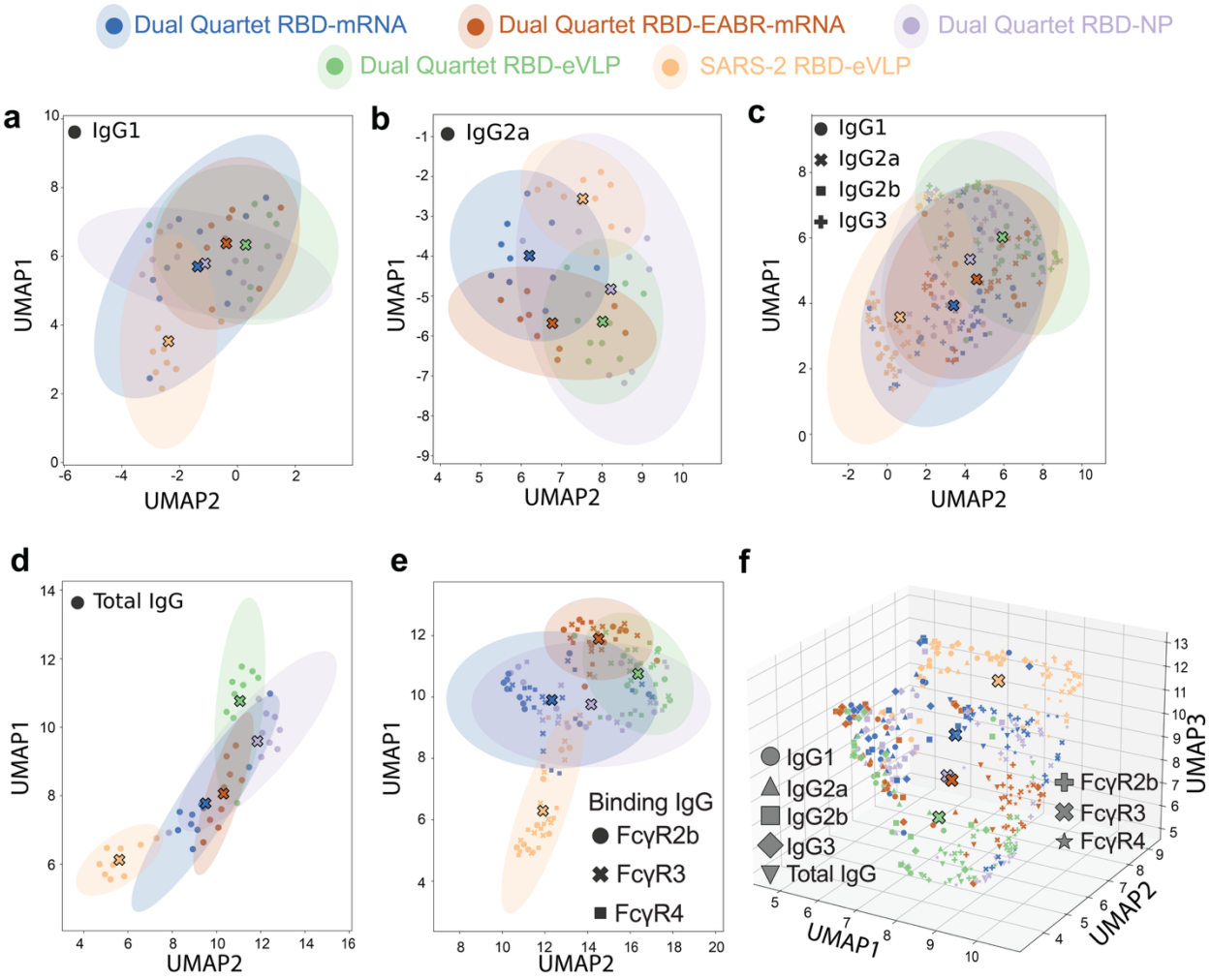

Figure 7. SySPEM UMAP analyses.
Uniform Manifold Approximation and Projection (UMAP)[55] was used to project multi-dimensional SySPEM scores into two (panels a-e) or three (panel f) dimensions for (a) IgG1 (b) IgG2a, (c) IgG1, IgG2a, IgG2b, and IgG3, (d) Total IgG, (e) FcγR-binding IgGs, and (f) Total IgG, FcγR-binding IgGs, and IgG subclasses. Samples with similar antibody–epitope recognition profiles cluster together, with colored ellipses indicating the variance within each immunogen group and centroid markers (large Xs) showing the group mean. (f) Three-dimensional UMAP projection for all IgG subclasses and FcγR-binding IgGs with centroid markers (large Xs). See also Fig. 6, Extended Data Figs. 6, 8.

Discussion

mRNA-based COVID-19 vaccines have been critical for preventing severe disease and death after SARS-2 infection[56], thereby helping to keep the worldwide pandemic in check. A recent modification of Moderna's mRNA-1273 vaccine involved changing the encoded antigen from a SARS-2 spike trimer to a membrane-bound spike N-terminal domain and RBD[57]. The new vaccine, mRNA-1283, exhibited equivalent or superior induced immune responses compared to mRNA-1273 in mice[57] and humans[58]. These results, together with the immunodominance of RBDs in SARS-2 infections and vaccinations[13], support further development of RBD-based COVID-19 and broader CoV vaccines.

We previously described protein-based RBD-NP immunogens that show promise as a pan-sarbecovirus vaccine[2-5,7,25,26]. However, manufacturing a protein-based mosaic-8 NP vaccine presents challenges. For example, mosaic-8 RBD-NP requires expression and purification of nine protein components (eight RBDs and a NP) to generate a conjugated RBD-NP, which then requires additional purification and characterization. mRNA vaccines offer the possibility of simpler manufacturing[59] but developing an mRNA vaccine that delivers eight individual RBD constructs would also be challenging, especially since mRNA delivery might not achieve co-display of all eight RBDs on cell surfaces and/or eVLPs.

Here, we report an efficient approach to develop an mRNA-encoded version of a broadly cross-reactive mosaic-8 RBD vaccine[2-5,7]. The new approach, inspired by protein-based dual quartet RBD-NPs[7], involves genetically encoding sarbecovirus RBDs arranged as two membrane-bound quartets, each comprising four tandemly arranged RBD ectodomains. RBD quartets offer the opportunity for optimal Ab induction by displaying a greater number of RBDs per transmembrane region compared with presentation of individual RBDs. The mRNA immunogens described here display dual RBD quartets at cell surfaces (dual quartet RBD-mRNA) or at both the surfaces of cells and secreted eVLPs (dual quartet RBD-EABR-mRNA) when an EABR cytoplasmic domain sequence is included[8]. Our analyses showed that dual quartet mRNA immunogens elicited equivalent or superior Ab responses, improved Fc effector functions, and increased T cell responses compared with protein-based dual quartet RBD-NPs. In addition, the dual quartet mRNA immunogens induced balanced T_H1/T_H2 responses, thereby stimulating both cellular and humoral immune responses. Thus, dual quartet RBD-mRNA immunogens retain the ability of conventional spike mRNA-LNP vaccines to activate cytotoxic CD8+ T cells and helper CD4+ T cells that can stimulate Ab-producing B cells[60]. Finally, and of critical importance for a potential pan-sarbecovirus vaccine, DMS experiments showed that mRNA-based dual RBD quartet immunogens induced Abs against conserved RBD epitopes, as required for a pan-sarbecovirus vaccine and as observed for protein-based mosaic-8 RBD-NP immunogens[2-5,7,25,26].

For characterizing dual quartet immunogens, we describe a new systems serology technique, SySPEM, that quantifies the degree of binding to individual epitopes on an antigen across IgG subclasses and FcγR-binding IgGs, therefore allowing for comparisons of epitope profiles elicited by different immunogens that are not possible using traditional systems serology[8]. SySPEM allows epitope mapping in a more indirect, but higher throughput, way than, e.g., electron microscopy-based EMPEM[61-64] but can deliver some of the same information while also delineating epitopes recognized by different Ab classes. In contrast to epitope mapping competition ELISAs[65], multiplexed SySPEM analyses use minimal sample volumes, do not rely on a panel of mAbs of known epitopes, and provide more precise epitope definition based on the location of added N-glycans. In the present study, SySPEM was used to show that the same antigen (dual quartet RBDs) delivered through mRNA- or protein-based vaccine modalities elicited distinct IgG class-specific

epitope profiles, suggesting that the way an antigen is presented can impact its epitope recognition by the immune system. Elucidating the mechanism by which this occurs warrants further study.

Here, SySPEM showed that, although overall binding and neutralizing Ab titers were similar, the dual quartet RBD-EABR-mRNA immunogen elicited stronger targeting of conserved class 4 and class 5 epitopes and weaker targeting of variable class 1/class 2 epitopes than the dual quartet RBD-mRNA immunogen, suggesting that the EABR approach could improve the effectiveness of an mRNA-encoded dual quartet RBD pan-sarbecovirus vaccine. For example, immunogen presentation on circulating eVLPs would promote wider antigen distribution to potentially engage larger populations of B cells[8,66]. Indeed, circulating RBD-eVLPs resulting from a dual quartet RBD-EABR-mRNA immunogen offer similar advantages to a recently described mRNA-delivered RBD protein nanoparticle[67] but also encode membrane-bound antigens at cell surfaces that could trigger additional immune responses. eVLP budding in the EABR approach might facilitate continuous replenishment of the cell surface with antigen, potentially increasing overall levels of antigen being displayed. The small size of eVLPs compared with a cell also facilitates efficient internalization by antigen-presenting cells[61-64], which could result in enhanced antigenic peptide presentation by class II MHC and activation of T follicular helper cells to promote B cell activation and germinal center formation[66]. Improvements for mRNA vaccines by including EABR appear to be general, as the EABR approach was shown to enhance vaccine-induced humoral responses against SARS-2[2-5,7], RSV[67], and influenza[22]. We also showed that a bivalent Wuhan-Hu-1/BA.5 spike-EABR-mRNA booster elicited more balanced targeting of multiple RBD epitopes in pre-vaccinated mice than conventional monovalent and bivalent spike-mRNA boosters, which primarily targeted variable RBD epitopes[66]. Taken together, our findings suggest that EABR-mRNA delivery of mosaic and multivalent immunogens improves targeting of conserved epitopes to enhance Ab breadth.

A pan-sarbecovirus vaccine candidate evaluated in mice would ideally elicit broad-binding IgG2a and IgG2b subclasses that promote robust Fc effector functions[49,50] to target conserved epitopes and elicit IgGs that bind to activating Fc receptors (FcγR3 and FcγR4). Using SySPEM, we show that dual RBD quartet immunogens, including the two mRNA-encoded versions, fulfill these criteria. There are many future potential applications for this new technology for design and evaluation of vaccines against a variety of viruses and other pathogens. For example, studies to establish correlates of protection of vaccines could include evaluations of SySPEM parameters to determine the relative protective effects of epitope targeting by different classes of IgGs, thus establishing desirable parameters for future vaccine efforts. In addition, SySPEM can be used to determine whether some epitopes elicit IgGs with different potential Fc effector functions, again to inform immunogen design for eliciting optimal immune responses against a particular pathogen.

In summary, our data support advancement of dual quartet RBD-mRNA immunogens into clinical development as a next-generation booster vaccine to provide protection from emerging SARS-2 variants and to reduce the chances of a future zoonotic sarbecovirus spillover from causing a new epidemic or pandemic.

Methods

Membrane-bound RBD quartet constructs

Sequences of the extracellular domains of RBD quartets 4a and 4b were based on previously reported SpyTag-Quartet (Genbank PP13603) and SpyTag-Alternate Quartet (GenBank PP136032, Addgene plasmid ID 214728) sequences[7]. mRNA constructs encoded a mouse Ig heavy chain signal peptide, codon-optimized RBD quartets 4a and 4b in which individual RBDs were separated by nine-residue Gly/Ser/Thr linkers followed by a five-residue Gly/Ser linker, the SARS-1 spike transmembrane domain, and a truncated spike cytoplasmic tail[68] (GenBank AAP13441.1, residues [1218-1235]). For RBD quartet 4a-EABR and 4b-EABR constructs, an endocytosis-preventing motif (EPM)[8], four-residue Gly/Ser linker, and the EABR[8] sequence were appended to the C-terminus. For in vitro assays, these constructs were cloned into the IVTpro T7 plasmid (Takara 6144), containing the immunogen open reading frame flanked by 5′ and 3′ untranslated regions (UTRs) and a genetically encoded poly(A) tail.

mRNA synthesis

For in vitro assays, IVTpro T7 plasmids encoding codon-optimized RBD quartet 4a, RBD quartet 4b, RBD quartet 4a-EABR, and RBD quartet 4b-EABR constructs were linearized by BspQI restriction digestion (NEB, R0712) and subsequently purified using the Zymo DNA Clean & Concentrator-25 kit (Zymo, D4034). mRNA was generated by in vitro transcription using the IVTpro™ T7 mRNA Synthesis Kit (Takara, 6144) following manufacturer's instructions, with the addition of the CleanCap Reagent AG (3' OMe) (TriLink, N-7413) and complete substitution of uridine with N1-Methylpseudouridine-5'-Triphosphate (TriLink, N-108; TriLink) to reduce immunogenicity[8]. mRNA was then purified by lithium chloride precipitation and an ethanol wash following standard protocols[69]. Purified mRNA was resuspended in nuclease-free water and stored at –80 °C.

For mRNAs used for in vivo immunization studies, constructs were synthesized by RNAcore (https://www.houstonmethodist.org/research-cores/rnacore/) using proprietary manufacturing protocols including incorporation of the CleanCap Reagent AG (3' OMe) (TriLink, N-7413) and complete substitution of uridine with N1-Methylpseudouridine-5'-Triphosphate (TriLink, N-108). mRNAs were purified by oligo-dT affinity purification. To remove double-stranded RNA contaminants, mRNAs were further purified using a cellulose-based method as described[70]. In brief, cellulose fibers (0.2 g/mL) were equilibrated in chromatography buffer (10mM HEPES pH 7.2, 0.1 mM EDTA, 125 mM NaCl, 16% ethanol) and added to microcentrifuge spin columns. mRNA diluted in chromatography buffer was added and shaken vigorously at room temperature for 30 minutes. The flow-through containing single-stranded mRNA was collected and purified with a sodium acetate precipitation and an ethanol wash. The final purified mRNA was filtered through a 0.2 µm filter before storage at –80 °C[8,70].

mRNA transfections and flow cytometry

HEK293T cells were seeded at 1×10^6 cells per well in 6-well plates and incubated for 20 h before transfection with 2 µg of mRNA encoding RBD quartet 4a, RBD quartet 4b, and/or their EABR-fused counterparts (4a-EABR, 4b-EABR) using Lipofectamine™ MessengerMax™ (Thermo Fisher Scientific). Forty-eight hours post-transfection, supernatants were collected for eVLP purification by ultracentrifugation on a 20 % sucrose cushion as described[8]. Cells were gently detached, resuspended in PBS+ (PBS + 2 % FBS), and 100 µL aliquots were taken for flow cytometry.

For the experiment shown in Extended Data Fig. 1a, cells were stained with the cross-reactive anti-RBD mAb C118[19,20] (2.5 µg/mL) for 30 min in the dark at room temperature, washed, and subsequently stained with Alexa Fluor® 647-conjugated anti-human IgG secondary antibody (Invitrogen, A21445; 1:4,000) for 15 min. After a final wash, cells were resuspended in PBS+ and analyzed on an Attune NxT Flow Cytometer (Thermo Fisher).

For the experiment shown in Extended Data Fig. 1c, cells were either singly transfected or co-transfected with combinations of RBD quartet 4a and 4b constructs and stained simultaneously with 2.5 µg/mL of Alexa Fluor® 647-conjugated anti-Rs4081 RBD[25] and Alexa Fluor® 488-conjugated M8a-7 IgG (anti-WIV1 RBD)[26] mAbs for 30 min at room temperature in the dark. After washing and resuspension, samples were analyzed on an Attune NxT Flow Cytometer. Results were plotted using FlowJo 10.5.3 software.

Production of dual quartet and SARS-2 RBD-eVLPs

Dual quartet RBD-eVLP and SARS-2 RBD-eVLP samples were generated as described[8] by transfecting Expi293F cells (Gibco) cultured in Expi293F expression media (Gibco) on an orbital shaker at 37°C and 8% CO_2. To generate dual quartet RBD-eVLPs, DNA plasmids encoding RBD quartet 4a-EABR and RBD quartet 4b-EABR constructs were mixed at a ratio of 1:1. 72 hours post-transfection, cells were centrifuged at 400 x g for 10 min, supernatants were passed through a 0.45 µm syringe filter and concentrated using Amicon Ultra-15 centrifugal filters with 100 kDa molecular weight cut-off (Millipore). eVLPs were purified by ultracentrifugation at 50,000 rpm (135,000 x g) for 2 hours at 4°C using a TLA100.3 rotor and an Optima™ TLX ultracentrifuge (Beckman Coulter) on a 20% w/v sucrose cushion. After removal of supernatants by aspiration, pellets were re-suspended in 200 µL sterile PBS at 4°C overnight. To remove residual debris, samples were centrifuged at 10,000 x g for 10 min, and supernatants were collected. eVLPs were further purified by SEC using a Superose 6 Increase 10/300 column (Cytiva) equilibrated with PBS. Peak fractions corresponding to eVLPs were combined and concentrated to 250-500 µL in Amicon Ultra-4 centrifugal filters with 100 kDa molecular weight cut-off. Samples were aliquoted and stored at -20°C.

The amount of SARS-2 RBD on SARS-2 RBD-eVLPs and the amount of dual quartet RBD on dual quartet RBD-eVLPs were determined by quantitative Western blot analysis. Various dilutions of SEC-purified eVLP samples and known amounts of either soluble SARS-2 RBD protein (Sino Biological, 40591-V08H-B-20) or purified soluble SpyTagged dual quartet RBDs (SpyTagged RBD quartets 4a and 4b were mixed at a ratio of 1:1) were separated by SDS-PAGE and transferred to nitrocellulose membranes (0.45 µm) (Thermo Fisher Scientific, LC2001). Rabbit anti-SARS-2 S1 polyclonal IgG (Thermo Fisher Scientific, PA5-116916; 1:1,000) and HRP-conjugated goat anti-rabbit IgG (Abcam, ab98467; 1:10,000) were used. Protein bands were visualized using ECL Prime Western Blotting Detection Reagent (Cytiva, RPN2232). Band intensities of the respective standards and eVLP sample dilutions were measured using ImageJ to determine RBD amounts.

LNP encapsulation of mRNAs

Purified dual quartet RBD-encoding mRNAs (RBD quartet 4a + RBD quartet 4b or RBD quartet 4a-EABR + RBD quartet 4b-EABR; 1:1 ratio) for in vivo studies were formulated in LNPs as previously described[71]. 1,2-distearoyl-*sn*-glycero-3-phosphocholine, cholesterol, a PEG lipid, and an ionizable cationic lipid dissolved in ethanol were rapidly mixed with an aqueous acidic solution containing mRNA using an in-line mixer. The ionizable lipid and LNP composition are described in the international patent application WO2017075531(2017). The post in-line solution was dialyzed with PBS to remove the ethanol and displace the acidic solution. LNP was measured for

size (60-65 nm) and polydispersity (PDI < 0.075) by dynamic light scattering (Malvern Nano ZS Zetasizer). Encapsulation efficiencies were >97% as measured by the Quant-iT Ribogreen Assay (Invitrogen).

Protein expression

RBDs, RBD quartets, and soluble sarbecovirus spike-6P[72] (SARS-2 WA1 and JN.1) or spike-2P (XBB.1.5, SARS-1, Rf1, Rs4091, Yun11, BM48-31, BtKY72) trimers were expressed as described[3,6,7]. Briefly, AviTag and/or His-tagged proteins were purified from transiently-transfected Expi293F cells (Gibco) by nickel affinity chromatography (HisTrap HP, Cytiva) and SEC (Superose 6 Increase 10/300, Cytiva)[3,44,73]. Fractions corresponding to proteins of interest were pooled, concentrated, and stored at 4ºC. Biotinylated proteins were generated as described[74] by co-transfection of AviTag/His-tagged spike and RBD constructs with a plasmid encoding an endoplasmic reticulum-directed BirA enzyme (kind gift from Michael Anaya, Caltech). The anti-Rs4081, anti-RmYN02, and anti-WIV1 RBD mAb IgGs from Extended Data Fig. 1 and the mAb IgGs and human ACE2-Fc protein shown in Extended Data Fig. 7c were expressed, purified, and classified as recognizing the RBD epitopes as described[20,25,26,44].

Preparation of RBD-NPs

For making dual quartet RBD-NPs, SpyCatcher003-mi3–C-Tag (Addgene 159995**)** subunits were expressed in BL21 (DE3) *E. coli* (Agilent) as described[75]. SpyCatcher003-mi3–C-Tag bacterial cell pellets were resuspended in 20 mL of 20 mM Tris-HCl pH 8.5, 300 mM NaCl, supplemented with 0.1 mg/mL lysozyme, 1 mg/mL cOmplete mini EDTA-free protease inhibitor (Roche), and 1.0 mM PMSF. After incubation at 4 °C for 45 min with end-over-end mixing, an Ultrasonic Processor equipped with a microtip (Cole-Parmer) was used to perform sonication on ice (four times for 60 s, 50% duty-cycle), and cell debris were cleared by centrifugation (35,000 x g for 45 min at 4 °C). SpyCatcher003-mi3–C-Tag was purified by ammonium sulfate precipitation (170 mg per mL of lysate) and resuspension, followed by SEC using a HiPrep Sephacryl S-400 HR 16-60 column (GE Healthcare) equilibrated with PBS as described[75]. Dual quartet RBD-NPs were generated by incubating purified SpyCatcher003-mi3–C-Tag with a 1:1 molar ratio of purified SpyTagged RBD quartets at 4 ºC in PBS.

Immunization of mice

Mouse procedures were approved by the Labcorp Institutional Animal Care and Use Committee. Six- to 7-week-old female BALB/c mice from Charles River Laboratories (RRID: IMSR_JAX:000664) were housed at Labcorp Drug Development, Denver, PA for immunizations. All animals were healthy upon receipt and monitored during a 7-day acclimation period. Mice were assigned randomly to experimental groups of 10 animals. Mouse cages were kept in a climate-controlled room (68 - 79 ºC) at 50 ± 20% relative humidity and provided with Rodent Diet #5001 (Purina Lab Diet) ad libitum.

Mice were immunized by intramuscular injection on days 0 and 28 with 1.5 or 0.5 µg dual quartet RBD-mRNA, 1.5 or 0.5 µg dual quartet RBD-EABR-mRNA, 5 µg dual quartet RBD-NP, 5 µg dual quartet RBD-eVLP, or 5 µg SARS-2 RBD-eVLP (based on RBD content for protein-based immunogens). Prior to immunizations, dual quartet RBD-NP, dual quartet RBD-eVLP, and SARS-2 RBD-eVLP immunogens were mixed with Addavax adjuvant (InvivoGen; 50% v/v). Serum samples for ELISAs and neutralization assays were obtained on indicated days by retro-orbital bleeding.

ELISAs

For eVLP sandwich ELISAs, 96-well high-binding plates (Corning, #9018) were coated overnight at 4 °C with capture monoclonal antibody (5 µg/mL in 0.1 M $NaHCO_3$, pH 9.8). Plates were blocked with 3% BSA and 0.1% Tween-20 in TBS (TBS-T) for 30 min at room temperature, followed by addition of serially diluted purified eVLP samples for 2 h. After washing, biotinylated detection antibodies (5 µg/mL in blocking buffer) were added for 2 h at room temperature. Plates were washed three times with TBS-T, incubated with streptavidin-HRP (Abcam, 7403; 1:20,000) for 30 min, washed again, and developed with 1-Step™ Ultra TMB-ELISA substrate solution (ThermoFisher). Reactions were stopped with 1 N HCl and absorbance was measured at 450 nm.

For the ELISA in Extended Data Fig. 1b, plates were coated with either anti-Rs4081[25] or anti-RmYN02[25] mAbs and detected with biotinylated C118[19,20]. For the ELISA in Extended Data Fig. 1d, plates were coated with anti-WIV1[26] and detected with biotinylated anti-Rs4081[25].

For serum ELISAs, purified His-tagged RBD (2.5 µg/mL in 0.1 M sodium bicarbonate buffer pH 9.8) was coated onto Nunc® MaxiSorp™ 384-wellplates (Sigma) and incubated overnight at 4˚C. After blocking with 3% bovine serum albumin (BSA), 0.1% Tween 20 in Tris-buffered saline (TBS-T) for 1 hour at room temperature, blocking solution was removed by aspiration. For serum ELISAs shown in Fig. 2 and Extended Data Fig. 2, mouse serum (1:100 initial dilution) was serially diluted by 3.1-fold in TBS-T/3% BSA and then added to plates for 3 hours at room temperature, followed by washing with TBS-T. Plates were then incubated for 1 hour with a 1:100,000 dilution of HRP-conjugated anti-IgG secondary (goat anti-mouse IgG; Abcam; RRID: AB_955439), and plates were washed with TBS-T. For mAb ELISAs shown in Extended Data Fig. 7, purified mAbs were serially diluted by 3.1-fold in TBS-T/3% BSA and then added to plates for 3 hours at room temperature, followed by washing with TBS-T. Plates were then incubated for 1 hour with a 1:100,000 dilution of HRP-conjugated anti-IgG secondary (goat anti-human IgG; SouthernBiotech 2014-05), and plates were washed with TBS-T. SuperSignal™ ELISA Femto Substrate (ThermoFisher) was added as per manufacturer's instructions, and luminescence was read at 425 nm. Data were collected in duplicate and midpoint titers (ED_{50} values) were obtained using Graphpad Prism 10.5.0 assuming a four-parameter dose-response curve fit.

Pseudovirus neutralization assays

Lentivirus-based pseudoviruses were produced in HEK293T cells (RRID:CVCL_0063) cultured in Dulbecco's modified Eagle's medium (DMEM, Gibco) supplemented with 10% heat-inactivated fetal bovine serum (FBS, Bio-Techne), 1% Penicillin/Streptomycin (Gibco), and 1% L-Glutamine (Gibco) at 37 °C and 5% CO_2. HEK293T-hACE2 cells (RRID:CVCL_A7UK)[43] and high-hACE2 HEK-293T (kindly provided by Kenneth Matreyek, Case Western Reserve University) target cells for neutralization assays were cultured in DMEM (Gibco) supplemented with 10% heat-inactivated FBS (Bio-Techne), 5 mg/mL gentamicin (Sigma-Aldrich), and 5 mg/mL blasticidin (Gibco) at 37 °C and 5% CO_2.

Lentiviral-based viruses were prepared as described[19,76] using genes encoding spike sequences lacking C-terminal residues in the cytoplasmic tail: deletions of 21 residues (SARS-2 variants) or 19 residues (SARS-1, Khosta-2-SARS-1 chimera, BtKY72-SARS-1 chimera). BtKY72 (containing K493Y/T498W substitutions) and Khosta-2 pseudoviruses were made with chimeric spikes in which the RBD from SARS-1 (residues 323-501) was substituted with the RBD from BtKY72 K493Y/T498W (residues 327-503) or Khosta-2 (residues 324-500) as described.[77]. Cells were co-transfected with HIV-1-based lentiviral plasmids, a luciferase reporter gene, and a coronavirus spike construct, resulting in lentivirus-based pseudovirions expressing a sarbecovirus

spike protein. Supernatants were harvested 48-72 hours post-transfection, filtered, and stored at -80 °C. Pseudovirus infectivity was determined by titration using HEK293T-hACE2 cells.

Prior to neutralization assays, serum from immunized mice was heat-inactivated at 56 ºC for 10 minutes. Heat-inactivated serum was three-fold serially diluted and incubated with pseudovirus for 1 hour at 37˚C, then the serum/virus mixture was added to HEK293T-hACE2 target cells or high-hACE2 HEK-293T cell line expressing hACE2 encoded with a consensus Kozak sequence (for SHC014 assays; kindly provided by Kenneth Matreyek, Case Western Reserve University) and incubated for 48 hours at 37ºC. After removing media, cells were lysed with Britelite Plus reagent (Revvity Health Sciences), and luciferase activity was measured as relative luminesce units (RLUs). Relative RLUs were normalized to RLUs from cells infected with pseudotyped virus in the absence of antiserum. Half-maximal inhibitory dilutions (ID_{50} values) were derived in AntibodyDatabase[78] using 4-parameter nonlinear regression.

ELISpot assays

Mice were euthanized on day 77 or 78, and spleens were collected and processed as described[8]. Briefly, spleens were homogenized using a gentleMACS Octo Dissociator (Miltenyi Biotec). Cells were passed through a 70 µm tissue screen, centrifuged at 1,500 rpm for 10 min, and resuspended in CTL-Test™ media (ImmunoSpot) containing 1% GlutaMAX™ supplement (Gibco). ELISpot assays were performed as described[8]. A SARS-CoV-2 spike PepMix™ pool of 315 peptides (15-mers with 11 amino acid overlap; JPT Peptide Technologies) was added to mouse IFNγ/IL4 double-color ELISpot plates (ImmunoSpot) at a concentration of 2 µg/mL, and 300,000 splenocytes were added per well. Plates were incubated at 37ºC for 24 hours. Biotinylated detection reagents, streptavidin-alkaline phosphatase (AP), and substrate reagents were added according to the manufacturer's guidelines. To stop the reactions, plates were gently rinsed with water three times. Plates were air-dried for two hours in a running laminar flow hood. Numbers of spots were quantified using a CTL ImmunoSpot S6 Universal-V Analyzer (Immunospot).

DMS Epitope Mapping

DMS experiments to map epitopes recognized by serum Abs were performed in biological duplicates using independent mutant RBD yeast libraries (WA1[79] and SARS-1[80] generously provided by Tyler Starr, University of Utah) as described[3,41]. Sera that had been heat inactivated for 30 min at 56 °C were incubated twice with 50 OD units of AWY101 yeast transformed with an empty vector in order to remove non-specific yeast-binding Abs. Expression of RBDs in libraries was induced in galactose-containing synthetic defined medium with Casamino acids (6.7g/L Yeast Nitrogen Base, 5.0 g/L Casamino acids, 1.065 g/L MES acid, and 2% w/v galactose plus 0.1% w/v dextrose). After 18 hours of induction, cells were washed twice and incubated with serum under conditions of gentle agitation for 1 hour at room temperature. Cells were labeled for 1 hour with a secondary Ab (1:200 Alexa Fluor-647-conjugated goat anti-mouse-IgG Fc-gamma, Jackson ImmunoResearch 115-605-008, RRID:AB_2338904) after washing twice.

Stained yeast cells were examined by fluorescence-activated cell sorting (FACS) using a Sony SH800 cell sorter. Cells were gated to capture RBD mutants that showed reduced Ab binding compared to a control. Cells were collected for each sample until ~5 x 10^6 RBD^+ cells were processed, which corresponds to ~5 x 10^5- 1 x 10^6 RBD^+ Ab-escaped cells. These cells were grown overnight in synthetic defined media (6.7 g/L Yeast Nitrogen Base, 5.0 g/L Casamino acids, 1.065 g/L MES acid, and 2% w/v dextrose, 100 U/mL penicillin, 100 µg/mL streptomycin) to expand cells prior to plasmid extraction. DNA extraction and Illumina sequencing were done as described[7] (raw sequencing data will be available on NCBI SRA). Escape fractions were computed as

described[7,41] using Swift DMS[7] (available upon request). Escape scores were calculated using a filter to remove variants with mutations that escaped binding because of poor expression, >1 amino acid mutation, or low sequencing counts[7,81].

Escape map visualizations (static line plots, logo plots, and structural depictions) were created using Swift DMS[7]. Line heights show the escape score for a particular amino acid substitution, as described[7]. In some visualizations, sites were categorized based on RBD epitope region[20,44-46]: class 1 (pink; RBD residues 403, 405, 406, 417, 420, 421, 453, 455-460, 473-478, 486, 487, 489, 503, 504); class 2 (purple; residues 472, 479, 483-485, 490-495), class 3 (blue; residues 341, 345, 346, 437-450, 496, 498-501,), class 4 (orange; residues 365-390, 408), class 5 (green; residues 352-357, 396, 462-468). In structural depictions of DMS results, an RBD surface (PDB 6M0J) was colored by the site-wise escape metric at each site, with red scaled at an escape fraction of 2.0. Residues exhibiting the highest escape fractions were labeled with their residue number, which was colored according to epitope class. Logo plot residues are colored according to RBD epitopes within different classes as indicated on the legend.

We stratified DMS escape fraction values into four groups. Escape fractions for each RBD substitution range from 0 (no cells with this substitution were sorted into the escape bin) to 1 (all cells with this substitution were sorted into the serum Ab escape bin)[40]. The sum of escape fractions for all substitutions at a specific site is represented by the total escape peak[40]. DMS profiles with total escape peaks <0.5 at all sites were classified as polyclass responses. DMS profiles with total escape peaks of 0.5 to 1, >1 to 2, or >2 at one or more sites were classified as weak, moderate, or strong escape profiles, respectively, corresponding to their RBD epitope (Table 1).

Systems serology: Ab subclass and FcγR binding profiling

Serum samples from immunized mice were analyzed in systems serology[9] experiments as described[6] using modifications of a Luminex assay to quantify the levels of antigen-specific Ab subclasses and FcγR binding profiles, which allows for simultaneous detection and quantification of multiple analytes (i.e., different antigens) in a single sample[82]. In brief, avidin (Sigma-Aldrich Catalog #: A9275-25MG) was coupled by carbodiimide-NHS ester chemistry to magnetic Luminex microspheres (LuminexCorp) using Sulfo-NHS (ThermoFisher™ Catalog number 24510) and 1-Ethyl-3-[3-dimethylaminopropyl]carbodiimide hydrochloride (EDC) (ThermoFisher™ Catalog number 22980) according to the manufacturer's instructions. Microspheres were blocked for 30 min with 1% BSA in PBS pH 7.4 (assay buffer) and then washed twice with PBS. Microspheres were incubated with biotinylated antigen (sarbecovirus spike trimer, RBD, or control antigen) at room temperature for 2 hours in assay buffer followed by blocking with 10 µM biotin (Millipore Sigma, Catalog B4501-100MG). Antigen-coupled microspheres were combined then incubated with heat-inactivated serum samples for 1 hour at room temperature in 96-well plates (Corning) at 1:200 or 1:1000 dilutions. Unbound IgGs were removed by washing twice with 200 µL of assay buffer. Total IgG was detected using a PE-conjugated secondary Ab recognizing mouse IgG (Southern Biotech 1030-09S). For evaluating antigen binding by different IgG subclasses, secondary Abs against mouse IgG subclasses (Southern Biotech 1070-09S, 1080-09S, 1090-09S, 1100-09S; PE-coupled anti-IgG1, IgG2a, IgG2b, IgG3) were added at a 1:1000 dilution in assay buffer and incubated for 1 hour with continuous shaking at room temperature. Excess primary and secondary Abs were removed by washing twice with 200 µL of assay buffer. Beads were resuspended in 200 µL of assay buffer, run in duplicate, and flowed in single file past two lasers on a Luminex™ FLEXMAP 3D™ Instrument System. In a Luminex assay, each bead region is impregnated with a different ratio of fluorescent dyes such that bead region identity, and

thereby antigen identity, is interrogated by the first laser. A second laser interrogates the signal of secondary Ab binding. Median fluorescence intensity (MFI) was calculated for all samples.

For evaluating FcγR-binding IgGs, soluble ectodomains of 6xHis-tagged FcγR2b, FcγR3, and FcγR4 were prepared as described[6] and biotinylated by co-expression with BirA enzyme in Expi293T cells[74]. Biotinylated FcγRs were purified on a HisTrap column (VWR) according to the manufacturer's instructions followed by SEC and then bound to PE-streptavidin (eBioscience). Labeled FcγRs were diluted 1:200 in assay buffer and incubated with serum-coated microspheres for 1 hour at room temperature with continuous shaking. Unbound primary and PE-labeled FcγR were removed as described for anti-IgG subclass secondary Abs. Beads were resuspended and run on a Luminex™ FLEXMAP 3D™ Instrument System to derive MFI values as described above.

Log_{10}-transformed heatmaps of antigen-specific IgG responses were generated using Python (v3.9.16) with the Pandas (v2.0.3), NumPy (v1.23.5), Matplotlib (v3.7.1), and Seaborn (v0.12.2) packages. A soluble influenza hemagglutinin trimer (listed as CA-09 HA in Fig. 5; expressed and purified as described[83]) was used as a control to evaluate non-specific binding.

SySPEM

One or more potential N-linked glycosylation site sequons (Asn-x-Ser/Thr)[84] were introduced at solvent-exposed residue(s) within the class 1 and class 2, class 2, class 3, class 4, class 1/4, or class 5 RBD epitopes[20,44-46] of the WA1 RBD (Extended Data Fig. 7a). Addition of N-glycan(s) was confirmed by SDS-PAGE as a shift in electrophoretic mobility to a higher apparent molecular weight (Extended Data Fig. 7b). Proper folding of RBD KO mutants and expected effects of added N-glycans were verified by assaying the binding of characterized mAbs or a human ACE2-Fc construct[20] by ELISA (Extended Data Fig. 7c). Binding of serum subsets to RBD wt and RBD KO proteins was measured using a Luminex multiplexed bead-based immunoassay as described above. The SySPEM score for each IgG sample/epitope pair was calculated as [1.0 – (RBD KO binding / RBD wt binding) x 100]. SySPEM scores range from limits of 100 (none of the IgGs in the sample bound to the RBD KO; i.e., all of the IgGs recognize the epitope that was targeted by the glycan addition) to 0 (all of the IgGs in the sample bound to the RBD KO; i.e., none of the IgGs recognize the epitope that was targeted by the glycan addition) (Extended Data Fig. 6). Python (v3.9.16) with the Pandas (v2.0.3), NumPy (v1.23.5), Matplotlib (v3.7.1), and Seaborn (v0.12.2) packages were used for box and whisker plots of SySPEM data. For UMAP visualizations in Fig. 7, SySPEM scores of each serum sample were organized into a feature matrix where each column contains an epitope class SySPEM score, and each row corresponds to an individual sample. Features were standardized using the standard scalar function on sckit-learn 1.4.2. UMAP was then performed with umap-learn (0.5.9.post2) on the standardized matrix. UMAP parameters: the nearest neighbors (n-neighbors) parameter was set to 12 and minimum distance (min-dist) was set to 0.25 to preserve the best local and global structures on the UMAP plot. Seaborn (v0.12.2) was used to plot resulting UMAPs.

Quantification and statistical analyses

We used pairwise comparisons, a method to evaluate sets of mean binding titers against individual viral strains for different immunization cohorts, as described previously[4] to determine if results from different immunized cohorts were significantly different from each other. For ELISAs and neutralizations (Fig. 2), we used analysis of variance (ANOVA) followed by Tukey's multiple comparison post hoc tests with the Geisser-Greenhouse correction, with pairing by viral strain, of ED_{50}s/ID_{50}s (converted to log_{10} scale) calculated using GraphPad Prism 10.5.0 to identify

statistically significant titer differences between immunized groups for ELISAs. For comparisons of neutralizing titers by strain (Extended Data Fig. 2), statistically significant titer differences between immunized groups for each given strain were determined using unpaired t test calculated using GraphPad Prism 10.5.0. For ELISpot assays, statistically significant differences between immunized cohorts were calculated using ordinary one-way ANOVA followed by Tukey's multiple comparison test using GraphPad Prism.

For statistical analysis of systems serology results, responses were aggregated by computing the geometric mean (geomean) across replicate samples for each immunogen-antigen combination. Log_{10}-transformed geomeans were compared across immunogen groups using Tukey's multiple comparison post hoc tests with the Geisser-Greenhouse correction, with pairing by viral strain calculated using GraphPad Prism 10.5.0. Box-and-whisker plots were generated for each IgG subclass or FcγR-binding IgG, displaying individual antigen-level geomeans per immunogen. Python (v3.9.16) with statsmodels (v0.14.4) packages were used for SySPEM Tukey's HSD posthoc statistical analyses. Statistical significance was annotated using brackets and asterisk notation ($p < 0.05$ *, $p < 0.01$ **, $p < 0.001$ ***, $p < 0.0001$ ****).

Materials, data, and code availability

DMS raw sequencing data will be available on the NCBI SRA under BioProject PRJNA1067836, BioSample when the NCBI SRA is back online. SySPEM scores for each IgG sample/epitope pair will be made publicly available upon publication. Materials are available upon request to corresponding authors with a signed material transfer agreement, and other information required to analyze the data in this paper is available from the lead contacts upon request. Code used for data processing and visualization of DMS, systems serology, and SySPEM results is available upon request.

Acknowledgements

We thank Annie Rorick, Han Gao, and Priyanthi Gnanapragasam for experimental assistance, Jesse Bloom (Fred Hutchinson Cancer Research Center) and Tyler Starr (University of Utah) for RBD libraries, Ryan McNamara and Galit Alter (Ragon Institute) for help with Systems Serology experiments, Jost Vielmetter, Luisa Segovia, Alyssa Player, Annie Lam, and the Caltech Beckman Institute Protein Expression Center for protein production, Igor Antoshechkin and the Caltech Millard and Muriel Jacobs Genetics and Genomics Laboratory for Illumina sequencing, Michael Anaya for help with Luminex experiments, Dom Aylard, Katie Lippert, and the Gladstone Flow Cytometry Core for help with flow cytometry, and Anthony West and Ying Tam (Acuitas) for critical reading of the manuscript. These studies were funded by Wellcome Leap (P.J.B.), the National Institutes of Health P01-AI165075 (P.J.B.), DP5OD033362 (M.A.G.H.), and 1K99AI185267 (A.A.C.), the Medical Research Council (MRC grant no. MR/Y011910/1 to M.R.H.), the Merkin Institute for Translational Research (Caltech) (P.J.B.), and the James B. Pendleton Charitable Trust that supports the Gladstone Flow Cytometry Core. This manuscript is the result of funding in whole or in part by the National Institutes of Health (NIH). It is subject to the NIH Public Access Policy. Through acceptance of this federal funding, NIH has been given a right to make this manuscript publicly available in PubMed Central upon the Official Date of Publication, as defined by NIH.

Author Contributions

Conceptualization: A.A.C., J.R.K., R.A.H., M.R.H., M.A.G.H., P.J.B.; Methodology: A.A.C., M.A.G.H.; Software: A.A.C.; Investigation: A.A.C., J.R.K., LM, IM, A.-C.P.F., K.-M.A.D., HES, M.A.G.H.; Resources: R.A.H., W.J.M., P.J.C.L.; Writing – original draft: A.A.C., J.R.K., K.-M.A.D., M.A.G.H., P.J.B.; Writing – review and editing: A.A.C., J.R.K., K.-M.A.D., R.A.H., M.R.H., M.A.G.H., P.J.B.; Visualization: A.A.C., J.R.K., K.-M.A.D., M.A.G.H., P.J.B.; Supervision: M.R.H., M.A.G.H., P.J.B.; Funding: M.A.G.H., P.J.B..

P.J.B. and A.A.C. are inventors on a US patent application (17/523,813) filed by the California Institute of Technology that covers mosaic RBD-NPs. M.A.G.H. and P.J.B. are inventors on a patent application (US17/835,751; international: PCT/US2022/032702) filed by the California Institute of Technology that covers the EABR technology. M.R.H. is an inventor on patents on spontaneous amide bond formation (EP2534484 and UK Intellectual Property Office 1706430.4) and a SpyBiotech co-founder and shareholder. P.J.B., M.A.G.H., A.A.C., J.R.K., K-M.A.D., R.A.H., and M.R.H. are co-inventors on a provisional US patent application filed by the California Institute of Technology that covers dual quartet mRNA immunogens. P.J.B. is a scientific advisor for Vaccine Company, Inc. M.A.G.H. is a scientific consultant for Vaccine Company, Inc. W.J.M. and P.J.C.L. are employees of Acuitas Therapeutics, a company developing LNP delivery technology; P.J.C.L. holds equity in Acuitas Therapeutics.

Literature cited

1 Whittaker, C., Barnsley, G., Mesa, D. O., Cox, V., Laydon, D. J., Tan, C. W., Zhu, F., Johnson, R., Doohan, P., Whittles, L. K., Nedjati-Gilani, G., Winskill, P., Hogan, A. B., Deol, A., Mukandavire, C., Hauck, K., Lye, D. C. B., Wang, L. F., Watson, O. J. & Ghani, A. C. Quantifying the impact of a broadly protective sarbecovirus vaccine in a future SARS-X pandemic. *Nat Commun* **16**, 8495 (2025).

2 Cohen, A. A., Gnanapragasam, P. N. P., Lee, Y. E., Hoffman, P. R., Ou, S., Kakutani, L. M., Keeffe, J. R., Wu, H. J., Howarth, M., West, A. P., Barnes, C. O., Nussenzweig, M. C. & Bjorkman, P. J. Mosaic nanoparticles elicit cross-reactive immune responses to zoonotic coronaviruses in mice. *Science* **371**, 735–741 (2021).

3 Cohen, A. A., van Doremalen, N., Greaney, A. J., Andersen, H., Sharma, A., Starr, T. N., Keeffe, J. R., Fan, C., Schulz, J. E., Gnanapragasam, P. N. P., Kakutani, L. M., West, A. P., Jr., Saturday, G., Lee, Y. E., Gao, H., Jette, C. A., Lewis, M. G., Tan, T. K., Townsend, A. R., Bloom, J. D., Munster, V. J. & Bjorkman, P. J. Mosaic RBD nanoparticles protect against challenge by diverse sarbecoviruses in animal models. *Science* **377**, eabq0839 (2022).

4 Cohen, A. A., Keeffe, J. R., Schiepers, A., Dross, S. E., Greaney, A. J., Rorick, A. V., Gao, H., Gnanapragasam, P. N. P., Fan, C., West, A. P., Jr., Ramsingh, A. I., Erasmus, J. H., Pata, J. D., Muramatsu, H., Pardi, N., Lin, P. J. C., Baxter, S., Cruz, R., Quintanar-Audelo, M., Robb, E., Serrano-Amatriain, C., Magneschi, L., Fotheringham, I. G., Fuller, D. H., Victora, G. D. & Bjorkman, P. J. Mosaic sarbecovirus nanoparticles elicit cross-reactive responses in pre-vaccinated animals. *Cell* **187**, 5554–5571 e5519 (2024).

5 Wang, E., Cohen, A. A., Caldera, L. F., Keeffe, J. R., Rorick, A. V., Adia, Y. M., Gnanapragasam, P. N. P., Bjorkman, P. J. & Chakraborty, A. K. Designed mosaic nanoparticles enhance cross-reactive immune responses in mice. *Cell* **188**, 1036–1050 e1011 (2025).

6 Cohen, A. A., Keeffe, J. R., Rorick, A. V., Rho, S., Priso Fils, A.-C., Manasyan, L., Gao, H., Gnanapragasam, P. N. P., Funke, H. H., Randolph, T. W., Garcea, R. L. & Bjorkman, P. J. Broad anti-sarbecovirus responses elicited by a single administration of mosaic-8 RBD-nanoparticle vaccine prepared using atomic layer deposition. *iScience* (2025).

7 Hills, R. A., Tan, T. K., Cohen, A. A., Keeffe, J. R., Keeble, A. H., Gnanapragasam, P. N. P., Storm, K. N., Rorick, A. V., West, A. P., Jr., Hill, M. L., Liu, S., Gilbert-Jaramillo, J., Afzal, M., Napier, A., Admans, G., James, W. S., Bjorkman, P. J., Townsend, A. R. & Howarth, M. R. Proactive vaccination using multiviral Quartet Nanocages to elicit broad anti-coronavirus responses. *Nat Nanotechnol* **19**, 1216–1223 (2024).

8 Hoffmann, M. A. G., Yang, Z., Huey-Tubman, K. E., Cohen, A. A., Gnanapragasam, P. N. P., Nakatomi, L. M., Storm, K. N., Moon, W. J., Lin, P. J. C., West, A. P., Jr. & Bjorkman, P. J. ESCRT recruitment to SARS-CoV-2 spike induces virus-like particles that improve mRNA vaccines. *Cell* **186**, 2380–2391 e2389 (2023).

9 Ackerman, M. E., Barouch, D. H. & Alter, G. Systems serology for evaluation of HIV vaccine trials. *Immunol Rev* **275**, 262–270 (2017).

10 Andersen, K. G., Rambaut, A., Lipkin, W. I., Holmes, E. C. & Garry, R. F. The proximal origin of SARS-CoV-2. *Nature Medicine* **26**, 450–452 (2020).

11 Roederer, A. L., Cao, Y., St Denis, K., Sheehan, M. L., Li, C. J., Lam, E. C., Gregory, D. J., Poznansky, M. C., Iafrate, A. J., Canaday, D. H., Gravenstein, S., Garcia-Beltran, W. F. & Balazs, A. B. Ongoing evolution of SARS-CoV-2 drives escape from mRNA vaccine-induced humoral immunity. *Cell Rep Med* **5**, 101850 (2024).

12 Hills, F. R., Geoghegan, J. L. & Bostina, M. Architects of infection: A structural overview of SARS-related coronavirus spike glycoproteins. *Virology* **604**, 110383 (2025).
13 Kleanthous, H., Silverman, J. M., Makar, K. W., Yoon, I. K., Jackson, N. & Vaughn, D. W. Scientific rationale for developing potent RBD-based vaccines targeting COVID-19. *NPJ Vaccines* **6**, 128 (2021).
14 Bruun, T. U. J., Andersson, A. C., Draper, S. J. & Howarth, M. Engineering a Rugged Nanoscaffold To Enhance Plug-and-Display Vaccination. *ACS Nano* **12**, 8855–8866 (2018).
15 Starr, T. N., Greaney, A. J., Hilton, S. K., Ellis, D., Crawford, K. H. D., Dingens, A. S., Navarro, M. J., Bowen, J. E., Tortorici, M. A., Walls, A. C., King, N. P., Veesler, D. & Bloom, J. D. Deep Mutational Scanning of SARS-CoV-2 Receptor Binding Domain Reveals Constraints on Folding and ACE2 Binding. *Cell* **182**, 1295–1310.e1220 (2020).
16 Gote, V., Bolla, P. K., Kommineni, N., Butreddy, A., Nukala, P. K., Palakurthi, S. S. & Khan, W. A Comprehensive Review of mRNA Vaccines. *Int J Mol Sci* **24** (2023).
17 Sievers, F., Wilm, A., Dineen, D., Gibson, T. J., Karplus, K., Li, W., Lopez, R., McWilliam, H., Remmert, M., Soding, J., Thompson, J. D. & Higgins, D. G. Fast, scalable generation of high-quality protein multiple sequence alignments using Clustal Omega. *Mol Syst Biol* **7**, 539 (2011).
18 Hou, X., Zaks, T., Langer, R. & Dong, Y. Lipid nanoparticles for mRNA delivery. *Nat Rev Mater*, 1–17 (2021).
19 Robbiani, D. F., Gaebler, C., Muecksch, F., Lorenzi, J. C. C., Wang, Z., Cho, A., Agudelo, M., Barnes, C. O., Gazumyan, A., Finkin, S., Hagglof, T., Oliveira, T. Y., Viant, C., Hurley, A., Hoffmann, H. H., Millard, K. G., Kost, R. G., Cipolla, M., Gordon, K., Bianchini, F., Chen, S. T., Ramos, V., Patel, R., Dizon, J., Shimeliovich, I., Mendoza, P., Hartweger, H., Nogueira, L., Pack, M., Horowitz, J., Schmidt, F., Weisblum, Y., Michailidis, E., Ashbrook, A. W., Waltari, E., Pak, J. E., Huey-Tubman, K. E., Koranda, N., Hoffman, P. R., West, A. P., Jr., Rice, C. M., Hatziioannou, T., Bjorkman, P. J., Bieniasz, P. D., Caskey, M. & Nussenzweig, M. C. Convergent antibody responses to SARS-CoV-2 in convalescent individuals. *Nature* **584**, 437–442 (2020).
20 Jette, C. A., Cohen, A. A., Gnanapragasam, P. N. P., Muecksch, F., Lee, Y. E., Huey-Tubman, K. E., Schmidt, F., Hatziioannou, T., Bieniasz, P. D., Nussenzweig, M. C., West, A. P., Keeffe, J. R., Bjorkman, P. J. & Barnes, C. O. Broad cross-reactivity across sarbecoviruses exhibited by a subset of COVID-19 donor-derived neutralizing antibodies. *Cell reports* **36**, 109760 (2021).
21 Votteler, J. & Sundquist, W. I. Virus budding and the ESCRT pathway. *Cell Host Microbe* **14**, 232–241 (2013).
22 Zhang, Y., Wang, C., Zheng, Y., Chen, F., Feng, Y., Fang, L., Wang, Z., Fu, Z. F., Zhou, M. & Zhao, L. A chimeric Ad5-Envp-VLP vaccine platform confers broad-spectrum 1 immunity against emerging and re-emerging pathogens *bioRxiv* (2025).
23 Gonzalez-Magaldi, M., Gullapalli, A., Papoulas, O., Liu, C., Leung, A. Y., Guo, L., Brilot, A. F., Marcotte, E. M., Ke, Z. & Leahy, D. J. Structure and organization of full-length epidermal growth factor receptor in extracellular vesicles by cryo-electron tomography. *Proc Natl Acad Sci U S A* **122**, e2424678122 (2025).
24 Olson, B. A., Huey-Tubman, K. E., Mao, Z., Hoffmann, M. A. G., Murray, R. M. & Mayo, S. L. Recruiting ESCRT to single-chain heterotrimer peptide-MHCI releases antigen-presenting vesicles that stimulate T cells selectively. (2025).
25 Fan, C., Keeffe, J. R., Malecek, K. E., Cohen, A. A., West, A. P., Jr., Baharani, V. A., Rorick, A. V., Gao, H., Gnanapragasam, P. N. P., Rho, S., Alvarez, J., Segovia, L. N., Hatziioannou, T., Bieniasz, P. D. & Bjorkman, P. J. Cross-reactive sarbecovirus antibodies

induced by mosaic RBD nanoparticles. *Proc Natl Acad Sci U S A* **122**, e2501637122 (2025).

26 Fan, C., Cohen, A. A., Park, M., Hung, A. F., Keeffe, J. R., Gnanapragasam, P. N. P., Lee, Y. E., Gao, H., Kakutani, L. M., Wu, Z., Kleanthous, H., Malecek, K. E., Williams, J. C. & Bjorkman, P. J. Neutralizing monoclonal antibodies elicited by mosaic RBD nanoparticles bind conserved sarbecovirus epitopes. *Immunity* **55**, 2419–2435 e2410 (2022).

27 Goldblatt, D., Alter, G., Crotty, S. & Plotkin, S. A. Correlates of protection against SARS-CoV-2 infection and COVID-19 disease. *Immunol Rev* **310**, 6–26 (2022).

28 Corbett, K. S., Nason, M. C., Flach, B., Gagne, M., O'Connell, S., Johnston, T. S., Shah, S. N., Edara, V. V., Floyd, K., Lai, L., McDanal, C., Francica, J. R., Flynn, B., Wu, K., Choi, A., Koch, M., Abiona, O. M., Werner, A. P., Moliva, J. I., Andrew, S. F., Donaldson, M. M., Fintzi, J., Flebbe, D. R., Lamb, E., Noe, A. T., Nurmukhambetova, S. T., Provost, S. J., Cook, A., Dodson, A., Faudree, A., Greenhouse, J., Kar, S., Pessaint, L., Porto, M., Steingrebe, K., Valentin, D., Zouantcha, S., Bock, K. W., Minai, M., Nagata, B. M., van de Wetering, R., Boyoglu-Barnum, S., Leung, K., Shi, W., Yang, E. S., Zhang, Y., Todd, J. M., Wang, L., Alvarado, G. S., Andersen, H., Foulds, K. E., Edwards, D. K., Mascola, J. R., Moore, I. N., Lewis, M. G., Carfi, A., Montefiori, D., Suthar, M. S., McDermott, A., Roederer, M., Sullivan, N. J., Douek, D. C., Graham, B. S. & Seder, R. A. Immune correlates of protection by mRNA-1273 vaccine against SARS-CoV-2 in nonhuman primates. *Science* **373**, eabj0299 (2021).

29 Gilbert, P. B., Montefiori, D. C., McDermott, A. B., Fong, Y., Benkeser, D., Deng, W., Zhou, H., Houchens, C. R., Martins, K., Jayashankar, L., Castellino, F., Flach, B., Lin, B. C., O'Connell, S., McDanal, C., Eaton, A., Sarzotti-Kelsoe, M., Lu, Y., Yu, C., Borate, B., van der Laan, L. W. P., Hejazi, N. S., Huynh, C., Miller, J., El Sahly, H. M., Baden, L. R., Baron, M., De La Cruz, L., Gay, C., Kalams, S., Kelley, C. F., Andrasik, M. P., Kublin, J. G., Corey, L., Neuzil, K. M., Carpp, L. N., Pajon, R., Follmann, D., Donis, R. O., Koup, R. A., Immune Assays Team section, s., Moderna, I. T. s. s., Coronavirus Vaccine Prevention Network /Coronavirus Efficacy Team section, s. & United States Government /Co, V. P. N. B. T. s. s. Immune correlates analysis of the mRNA-1273 COVID-19 vaccine efficacy clinical trial. *Science* **375**, 43–50 (2022).

30 Schmidt, F., Weisblum, Y., Muecksch, F., Hoffmann, H.-H., Michailidis, E., Lorenzi, J. C. C., Mendoza, P., Rutkowska, M., Bednarski, E., Gaebler, C., Agudelo, M., Cho, A., Wang, Z., Gazumyan, A., Cipolla, M., Caskey, M., Robbiani, D. F., Nussenzweig, M. C., Rice, C. M., Hatziioannou, T. & Bieniasz, P. D. Measuring SARS-CoV-2 neutralizing antibody activity using pseudotyped and chimeric viruses. *Journal of Experimental Medicine* **217** (2020).

31 Corbett, K. S., Edwards, D. K., Leist, S. R., Abiona, O. M., Boyoglu-Barnum, S., Gillespie, R. A., Himansu, S., Schafer, A., Ziwawo, C. T., DiPiazza, A. T., Dinnon, K. H., Elbashir, S. M., Shaw, C. A., Woods, A., Fritch, E. J., Martinez, D. R., Bock, K. W., Minai, M., Nagata, B. M., Hutchinson, G. B., Wu, K., Henry, C., Bahl, K., Garcia-Dominguez, D., Ma, L., Renzi, I., Kong, W. P., Schmidt, S. D., Wang, L., Zhang, Y., Phung, E., Chang, L. A., Loomis, R. J., Altaras, N. E., Narayanan, E., Metkar, M., Presnyak, V., Liu, C., Louder, M. K., Shi, W., Leung, K., Yang, E. S., West, A., Gully, K. L., Stevens, L. J., Wang, N., Wrapp, D., Doria-Rose, N. A., Stewart-Jones, G., Bennett, H., Alvarado, G. S., Nason, M. C., Ruckwardt, T. J., McLellan, J. S., Denison, M. R., Chappell, J. D., Moore, I. N., Morabito, K. M., Mascola, J. R., Baric, R. S., Carfi, A. & Graham, B. S. SARS-CoV-2 mRNA vaccine design enabled by prototype pathogen preparedness. *Nature* **586**, 567–571 (2020).

32 Paciello, I., Maccari, G., Pantano, E., Andreano, E. & Rappuoli, R. High-resolution map of the Fc functions mediated by COVID-19-neutralizing antibodies. *Proc Natl Acad Sci U S A* **121**, e2314730121 (2024).

33 Abu-Humaidan, A. H. A., Ahmad, F. M., Awajan, D., Jarrar, R. F. & Alaridah, N. Anti-SARS-Cov-2 S-RBD IgG Formed after BNT162b2 Vaccination Can Bind C1q and Activate Complement. *J Immunol Res* **2022**, 7263740 (2022).

34 Clark, J. J., Hoxie, I., Adelsberg, D. C., Sapse, I. A., Andreata-Santos, R., Yong, J. S., Amanat, F., Tcheou, J., Raskin, A., Singh, G., Gonzalez-Dominguez, I., Edgar, J. E., Bournazos, S., Sun, W., Carreno, J. M., Simon, V., Ellebedy, A. H., Bajic, G. & Krammer, F. Protective effect and molecular mechanisms of human non-neutralizing cross-reactive spike antibodies elicited by SARS-CoV-2 mRNA vaccination. *Cell reports* **43**, 114922 (2024).

35 Ranieri, E., Popescu, I. & Gigante, M. CTL ELISPOT assay. *Methods Mol Biol* **1186**, 75–86 (2014).

36 Leehan, K. M. & Koelsch, K. A. T Cell ELISPOT: For the Identification of Specific Cytokine-Secreting T Cells. *Methods Mol Biol* **1312**, 427–434 (2015).

37 Rock, K. L., Reits, E. & Neefjes, J. Present Yourself! By MHC Class I and MHC Class II Molecules. *Trends Immunol* **37**, 724–737 (2016).

38 Greaney, A. J., Loes, A. N., Crawford, K. H. D., Starr, T. N., Malone, K. D., Chu, H. Y. & Bloom, J. D. Comprehensive mapping of mutations in the SARS-CoV-2 receptor-binding domain that affect recognition by polyclonal human plasma antibodies. *Cell Host Microbe* **29**, 463–476 e466 (2021).

39 Greaney, A. J., Loes, A. N., Gentles, L. E., Crawford, K. H. D., Starr, T. N., Malone, K. D., Chu, H. Y. & Bloom, J. D. Antibodies elicited by mRNA-1273 vaccination bind more broadly to the receptor binding domain than do those from SARS-CoV-2 infection. *Science translational medicine* **13** (2021).

40 Greaney, A. J., Starr, T. N., Barnes, C. O., Weisblum, Y., Schmidt, F., Caskey, M., Gaebler, C., Cho, A., Agudelo, M., Finkin, S., Wang, Z., Poston, D., Muecksch, F., Hatziioannou, T., Bieniasz, P. D., Robbiani, D. F., Nussenzweig, M. C., Bjorkman, P. J. & Bloom, J. D. Mapping mutations to the SARS-CoV-2 RBD that escape binding by different classes of antibodies. *Nat Commun* **12**, 4196 (2021).

41 Greaney, A. J., Starr, T. N., Gilchuk, P., Zost, S. J., Binshtein, E., Loes, A. N., Hilton, S. K., Huddleston, J., Eguia, R., Crawford, K. H. D., Dingens, A. S., Nargi, R. S., Sutton, R. E., Suryadevara, N., Rothlauf, P. W., Liu, Z., Whelan, S. P. J., Carnahan, R. H., Crowe, J. E., Jr. & Bloom, J. D. Complete Mapping of Mutations to the SARS-CoV-2 Spike Receptor-Binding Domain that Escape Antibody Recognition. *Cell Host Microbe* **29**, 44–57 e49 (2021).

42 Starr, T. N., Czudnochowski, N., Liu, Z., Zatta, F., Park, Y. J., Addetia, A., Pinto, D., Beltramello, M., Hernandez, P., Greaney, A. J., Marzi, R., Glass, W. G., Zhang, I., Dingens, A. S., Bowen, J. E., Tortorici, M. A., Walls, A. C., Wojcechowskyj, J. A., De Marco, A., Rosen, L. E., Zhou, J., Montiel-Ruiz, M., Kaiser, H., Dillen, J. R., Tucker, H., Bassi, J., Silacci-Fregni, C., Housley, M. P., di Iulio, J., Lombardo, G., Agostini, M., Sprugasci, N., Culap, K., Jaconi, S., Meury, M., Dellota, E., Jr., Abdelnabi, R., Foo, S. C., Cameroni, E., Stumpf, S., Croll, T. I., Nix, J. C., Havenar-Daughton, C., Piccoli, L., Benigni, F., Neyts, J., Telenti, A., Lempp, F. A., Pizzuto, M. S., Chodera, J. D., Hebner, C. M., Virgin, H. W., Whelan, S. P. J., Veesler, D., Corti, D., Bloom, J. D. & Snell, G. SARS-CoV-2 RBD antibodies that maximize breadth and resistance to escape. *Nature* **597**, 97–102 (2021).

43 Starr, T. N., Greaney, A. J., Addetia, A., Hannon, W. W., Choudhary, M. C., Dingens, A. S., Li, J. Z. & Bloom, J. D. Prospective mapping of viral mutations that escape antibodies used to treat COVID-19. *Science* **371**, 850–854 (2021).

44 Barnes, C. O., Jette, C. A., Abernathy, M. E., Dam, K.-M. A., Esswein, S. R., Gristick, H. B., Malyutin, A. G., Sharaf, N. G., Huey-Tubman, K. E., Lee, Y. E., Robbiani, D. F., Nussenzweig, M. C., West, A. P. & Bjorkman, P. J. SARS-CoV-2 neutralizing antibody structures inform therapeutic strategies. *Nature* **588**, 682–687 (2020).

45 Jensen, J. L., Sankhala, R. S., Dussupt, V., Bai, H., Hajduczki, A., Lal, K. G., Chang, W. C., Martinez, E. J., Peterson, C. E., Golub, E. S., Rees, P. A., Mendez-Rivera, L., Zemil, M., Kavusak, E., Mayer, S. V., Wieczorek, L., Kannan, S., Doranz, B. J., Davidson, E., Yang, E. S., Zhang, Y., Chen, M., Choe, M., Wang, L., Gromowski, G. D., Koup, R. A., Michael, N. L., Polonis, V. R., Rolland, M., Modjarrad, K., Krebs, S. J. & Joyce, M. G. Targeting the Spike Receptor Binding Domain Class V Cryptic Epitope by an Antibody with Pan-Sarbecovirus Activity. *J Virol* **97**, e0159622 (2023).

46 Cui, L., Li, T., Lan, M., Zhou, M., Xue, W., Zhang, S., Wang, H., Hong, M., Zhang, Y., Yuan, L., Sun, H., Ye, J., Zheng, Q., Guan, Y., Gu, Y., Xia, N. & Li, S. A cryptic site in class 5 epitope of SARS-CoV-2 RBD maintains highly conservation across natural isolates. *iScience* **27**, 110208 (2024).

47 Bangaru, S., Jackson, A. M., Copps, J., Fernandez-Quintero, M. L., Torres, J. L., Richey, S. T., Nogal, B., Sewall, L. M., Torrents de la Pena, A., Rehman, A., Guebre-Xabier, M., Girard, B., Das, R., Corbett-Helaire, K. S., Seder, R. A., Graham, B. S., Edwards, D. K., Patel, N., Smith, G. & Ward, A. B. Structural serology of polyclonal antibody responses to mRNA-1273 and NVX-CoV2373 COVID-19 vaccines. *Cell reports* **44**, 115986 (2025).

48 Landau, M., Mayrose, I., Rosenberg, Y., Glaser, F., Martz, E., Pupko, T. & Ben-Tal, N. ConSurf 2005: the projection of evolutionary conservation scores of residues on protein structures. *Nucleic Acids Res* **33**, W299–302 (2005).

49 Crescioli, S., Jatiani, S. & Moise, L. With great power, comes great responsibility: the importance of broadly measuring Fc-mediated effector function early in the antibody development process. *MAbs* **17**, 2453515 (2025).

50 Bruhns, P. & Jonsson, F. Mouse and human FcR effector functions. *Immunol Rev* **268**, 25–51 (2015).

51 Hwang, H. S., Lee, Y. T., Kim, K. H., Seo, H. S., Yang, K. S., Cho, H. & Kang, S. M. Roles of the Fc Receptor gamma-Chain in Inducing Protective Immune Responses after Heterologous Vaccination against Respiratory Syncytial Virus Infection. *Vaccines (Basel)* **9** (2021).

52 Aleebrahim-Dehkordi, E., Molavi, B., Mokhtari, M., Deravi, N., Fathi, M., Fazel, T., Mohebalizadeh, M., Koochaki, P., Shobeiri, P. & Hasanpour-Dehkordi, A. T helper type (Th1/Th2) responses to SARS-CoV-2 and influenza A (H1N1) virus: From cytokines produced to immune responses. *Transplant Immunology* **70** (2022).

53 Han, Q., Gao, X., Chu, Z., Wang, X., Eisa Addoma Adam, F., Zhang, S., Jia, Y., Qiu, X., Wang, X. & Yang, Z. Truncated chicken MDA5 enhances the immune response to inactivated NDV vaccine. *Vet Immunol Immunopathol* **208**, 44–52 (2019).

54 Turner, H. L., Jackson, A. M., Richey, S. T., Sewall, L. M., Antanasijevic, A., Hangartner, L. & Ward, A. B. Protocol for analyzing antibody responses to glycoprotein antigens using electron-microscopy-based polyclonal epitope mapping. *STAR Protoc* **4**, 102476 (2023).

55 McInnes, L., Healy, J. & Melville, J. *UMAP: Uniform Manifold Approximation and Projection for Dimension Reduction, v3*, <https://arxiv.org/abs/1802.03426v3> (2020).

56 Wong, B. K. & Mabbott, N. A. Systematic review and meta-analysis of COVID-19 mRNA vaccine effectiveness against hospitalizations in adults. *Immunother Adv* **4**, ltae011 (2024).

57 Stewart-Jones, G. B. E., Elbashir, S. M., Wu, K., Lee, D., Renzi, I., Ying, B., Koch, M., Sein, C. E., Choi, A., Whitener, B., Garcia-Dominguez, D., Henry, C., Woods, A., Ma, L., Montes Berrueta, D., Avena, L. E., Quinones, J., Falcone, S., Hsiao, C. J., Scheaffer, S. M., Thackray, L. B., White, P., Diamond, M. S., Edwards, D. K. & Carfi, A. Domain-based mRNA vaccines encoding spike protein N-terminal and receptor binding domains confer protection against SARS-CoV-2. *Science translational medicine* **15**, eadf4100 (2023).

58 Chalkias, S., Dennis, P., Petersen, D., Radhakrishnan, K., Vaughan, L., Handforth, R., Rossi, A., Wahid, R., Edwards, D. K., Feng, J., Deng, W., Zhou, H., De Windt, E., Urdaneta, V., Paila, Y., Girard, B., Faust, S. N., Walsh, S. R., Cosgrove, C. A., Miller, J. & Das, R. Efficacy, immunogenicity, and safety of a next-generation mRNA-1283 COVID-19 vaccine compared with the mRNA-1273 vaccine (NextCOVE): results from a phase 3, randomised, observer-blind, active-controlled trial. *The Lancet Infectious Diseases* (2025).

59 Pardi, N., Hogan, M. J., Porter, F. W. & Weissman, D. mRNA vaccines - a new era in vaccinology. *Nat Rev Drug Discov* **17**, 261–279 (2018).

60 Mahrokhian, S. H., Tostanoski, L. H., Vidal, S. J. & Barouch, D. H. COVID-19 vaccines: Immune correlates and clinical outcomes. *Hum Vaccin Immunother* **20**, 2324549 (2024).

61 Foged, C., Brodin, B., Frokjaer, S. & Sundblad, A. Particle size and surface charge affect particle uptake by human dendritic cells in an in vitro model. *Int J Pharm* **298**, 315–322 (2005).

62 Joshi, V. B., Geary, S. M. & Salem, A. K. Biodegradable particles as vaccine delivery systems: size matters. *AAPS J* **15**, 85–94 (2013).

63 Zepeda-Cervantes, J., Ramirez-Jarquin, J. O. & Vaca, L. Interaction Between Virus-Like Particles (VLPs) and Pattern Recognition Receptors (PRRs) From Dendritic Cells (DCs): Toward Better Engineering of VLPs. *Front Immunol* **11**, 1100 (2020).

64 Kim, C., Kim, J. D. & Seo, S. U. Nanoparticle and virus-like particle vaccine approaches against SARS-CoV-2. *J Microbiol* **60**, 335–346 (2022).

65 Morris, G. E. in *The Protein Protocols Handbook Springer Protocols Handbooks* Ch. Chapter 96, 595–600 (1996).

66 Fan, C., Cohen, A. A., Dam, K. A., Rorick, A. V., Priso Fils, A. I., Yang, Z., Gnanapragasam, P. N. P., Segovia, L. N., Huey-Tubman, K. E., Moon, W. J., Lin, P. J. C., Bjorkman, P. J. & Hoffmann, M. A. G. Bivalent mRNA booster encoding virus-like particles elicits potent polyclass RBD antibodies in pre-vaccinated mice. *bioRxiv* (2025).

67 Chai, P., Shi, Y., Li, X., Yang, M., Liu, X., Liu, M., Yu, J., Yin, X., Li, D., Li, K., Kong, X., Zhang, Q., Wang, H., Sun, X., Li, J., Li, L., Li, D., Pang, L., Lu, X. & Duan, Z. Improved mRNA-based RSV vaccine with PreF forming enveloped virus-like particles. *NPJ Vaccines* **10**, 152 (2025).

68 McBride, C. E., Li, J. & Machamer, C. E. The cytoplasmic tail of the severe acute respiratory syndrome coronavirus spike protein contains a novel endoplasmic reticulum retrieval signal that binds COPI and promotes interaction with membrane protein. *J Virol* **81**, 2418–2428 (2007).

69 Walker, S. E. & Lorsch, J. RNA purification--precipitation methods. *Methods Enzymol* **530**, 337–343 (2013).

70 Baiersdorfer, M., Boros, G., Muramatsu, H., Mahiny, A., Vlatkovic, I., Sahin, U. & Kariko, K. A Facile Method for the Removal of dsRNA Contaminant from In Vitro-Transcribed mRNA. *Mol Ther Nucleic Acids* **15**, 26–35 (2019).

71 Pardi, N., Tuyishime, S., Muramatsu, H., Kariko, K., Mui, B. L., Tam, Y. K., Madden, T. D., Hope, M. J. & Weissman, D. Expression kinetics of nucleoside-modified mRNA

delivered in lipid nanoparticles to mice by various routes. *J Control Release* **217**, 345–351 (2015).

72 Hsieh, C. L., Goldsmith, J. A., Schaub, J. M., DiVenere, A. M., Kuo, H. C., Javanmardi, K., Le, K. C., Wrapp, D., Lee, A. G., Liu, Y., Chou, C. W., Byrne, P. O., Hjorth, C. K., Johnson, N. V., Ludes-Meyers, J., Nguyen, A. W., Park, J., Wang, N., Amengor, D., Lavinder, J. J., Ippolito, G. C., Maynard, J. A., Finkelstein, I. J. & McLellan, J. S. Structure-based design of prefusion-stabilized SARS-CoV-2 spikes. *Science* **369**, 1501–1505 (2020).

73 Wang, Z., Muecksch, F., Cho, A., Gaebler, C., Hoffmann, H. H., Ramos, V., Zong, S., Cipolla, M., Johnson, B., Schmidt, F., DaSilva, J., Bednarski, E., Ben Tanfous, T., Raspe, R., Yao, K., Lee, Y. E., Chen, T., Turroja, M., Milard, K. G., Dizon, J., Kaczynska, A., Gazumyan, A., Oliveira, T. Y., Rice, C. M., Caskey, M., Bieniasz, P. D., Hatziioannou, T., Barnes, C. O. & Nussenzweig, M. C. Analysis of memory B cells identifies conserved neutralizing epitopes on the N-terminal domain of variant SARS-Cov-2 spike proteins. *Immunity* **55**, 998–1012 e1018 (2022).

74 Tykvart, J., Sacha, P., Barinka, C., Knedlik, T., Starkova, J., Lubkowski, J. & Konvalinka, J. Efficient and versatile one-step affinity purification of in vivo biotinylated proteins: expression, characterization and structure analysis of recombinant human glutamate carboxypeptidase II. *Protein Expr Purif* **82**, 106–115 (2012).

75 Rahikainen, R., Rijal, P., Tan, T. K., Wu, H. J., Andersson, A. C., Barrett, J. R., Bowden, T. A., Draper, S. J., Townsend, A. R. & Howarth, M. Overcoming Symmetry Mismatch in Vaccine Nanoassembly through Spontaneous Amidation. *Angew Chem Int Ed Engl* **60**, 321–330 (2021).

76 Crawford, K. H. D., Eguia, R., Dingens, A. S., Loes, A. N., Malone, K. D., Wolf, C. R., Chu, H. Y., Tortorici, M. A., Veesler, D., Murphy, M., Pettie, D., King, N. P., Balazs, A. B. & Bloom, J. D. Protocol and Reagents for Pseudotyping Lentiviral Particles with SARS-CoV-2 Spike Protein for Neutralization Assays. *Viruses* **12** (2020).

77 Seifert, S. N., Bai, S., Fawcett, S., Norton, E. B., Zwezdaryk, K. J., Robinson, J., Gunn, B. & Letko, M. An ACE2-dependent Sarbecovirus in Russian bats is resistant to SARS-CoV-2 vaccines. *PLoS Pathog* **18**, e1010828 (2022).

78 West, A. P., Jr., Scharf, L., Horwitz, J., Klein, F., Nussenzweig, M. C. & Bjorkman, P. J. Computational analysis of anti-HIV-1 antibody neutralization panel data to identify potential functional epitope residues. *Proc Natl Acad Sci U S A* **110**, 10598–10603 (2013).

79 Starr, T. N., Greaney, A. J., Hannon, W. W., Loes, A. N., Hauser, K., Dillen, J. R., Ferri, E., Farrell, A. G., Dadonaite, B., McCallum, M., Matreyek, K. A., Corti, D., Veesler, D., Snell, G. & Bloom, J. D. Shifting mutational constraints in the SARS-CoV-2 receptor-binding domain during viral evolution. *Science* **377**, 420–424 (2022).

80 Lee, J., Zepeda, S. K., Park, Y. J., Taylor, A. L., Quispe, J., Stewart, C., Leaf, E. M., Treichel, C., Corti, D., King, N. P., Starr, T. N. & Veesler, D. Broad receptor tropism and immunogenicity of a clade 3 sarbecovirus. *Cell Host Microbe* **31**, 1961–1973 e1911 (2023).

81 Greaney, A. J., Starr, T. N., Eguia, R. T., Loes, A. N., Khan, K., Karim, F., Cele, S., Bowen, J. E., Logue, J. K., Corti, D., Veesler, D., Chu, H. Y., Sigal, A. & Bloom, J. D. A SARS-CoV-2 variant elicits an antibody response with a shifted immunodominance hierarchy. *PLoS Pathog* **18**, e1010248 (2022).

82 Brown, E. P., Dowell, K. G., Boesch, A. W., Normandin, E., Mahan, A. E., Chu, T., Barouch, D. H., Bailey-Kellogg, C., Alter, G. & Ackerman, M. E. Multiplexed Fc array for evaluation of antigen-specific antibody effector profiles. *J Immunol Methods* **443**, 33–44 (2017).

83 Cohen, A. A., Yang, Z., Gnanapragasam, P. N. P., Ou, S., Dam, K. A., Wang, H. & Bjorkman, P. J. Construction, characterization, and immunization of nanoparticles that display a diverse array of influenza HA trimers. *PLoS One* **16**, e0247963 (2021).

84 Lehle, L. & Bause, E. Primary structural requirements for N- and O-glycosylation of yeast mannoproteins. *Biochimica et Biophysica Acta (BBA) - General Subjects* **799**, 246–251 (1984).

Supplementary Information for

Genetic encoding of mosaic-8 pan-sarbecovirus RBD vaccine for mRNA delivery

Alexander A. Cohen[1], Jennifer R. Keeffe[1], Lusineh Manasyan[1], Indeever Madireddy[1], Ange-Célia I. Priso Fils[1], Kim-Marie A. Dam[2], Haley E. Stober[2], Rory A. Hills[3,4,7], Woohyun J. Moon[5], Paulo J.C. Lin[5], Mark R. Howarth[3], Magnus A.G. Hoffmann[2,6,8*], Pamela J. Bjorkman[1,8*]

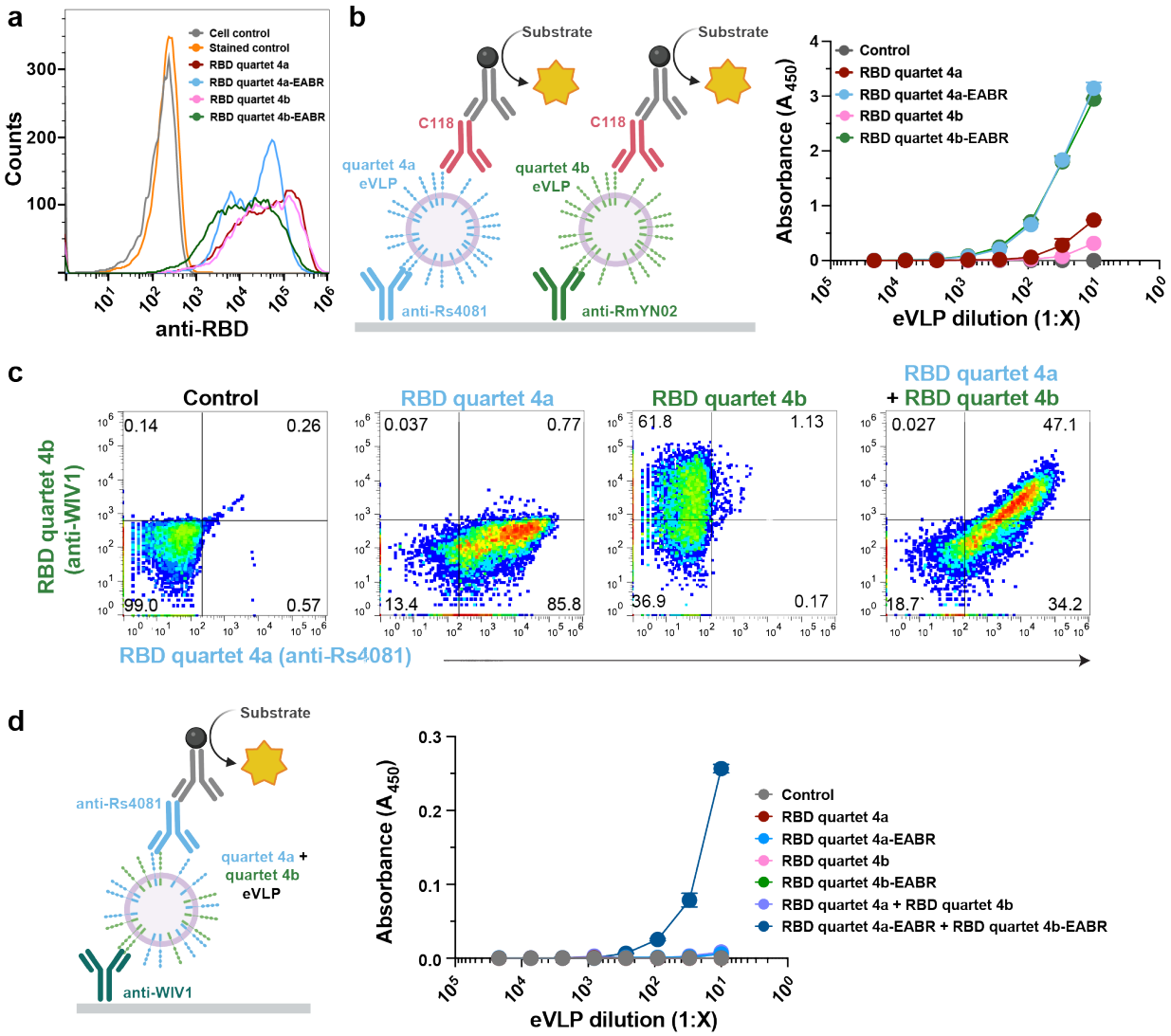

Extended Data Figure 1. mRNA-encoded dual quartets are presented on cells and eVLPs. (a) Flow cytometry using C118, a human pan-sarbecovirus RBD-specific mAb[19,20], demonstrating that transfections of mRNAs encoding EABR and non-EABR versions of RBD quartet 4a or quartet 4b resulted in expression on the surface of transfected cells. Untransfected cells are shown as controls (unstained or stained with C118). (b) Left: ELISA schematic. RBD quartet levels were measured by capturing purified eVLPs with an anti-Rs4081 RBD mAb[25] (recognizes RBD quartet 4a but not quartet 4b) or an anti-RmYN02 RBD mAb[25] (recognizes RBD quartet 4b but not quartet 4a) and detecting with the pan-sarbecovirus RBD-specific C118 mAb[19,20]. Right: ELISA showing that purified single quartet eVLPs purified from supernatants of cells transfected with mRNA encoding RBD quartet 4a-EABR or RBD quartet 4b-EABR displayed RBD quartets on their surface. The mean absorbance of two replicates is shown as a function of eVLP dilution with error bars representing standard deviations. (c) Flow cytometry demonstrating that RBD quartets 4a and 4b were co-expressed on the surfaces of individual cells. RBD quartet 4a was detected using an anti-Rs4081 RBD mAb[25] and RBD quartet 4b was detected using anti-WIV1 RBD mAb[26]. Untransfected cells stained with the anti-Rs4081 and anti-WIV1 RBD mAbs are shown as controls. The percentage of cells in each quadrant is shown. (d) Left: ELISA schematic. Purified eVLPs were evaluated in a sandwich ELISA in which an anti-WIV1 RBD mAb[26] (recognizes RBD quartet 4b but not quartet 4a) was used as a capture Ab and an anti-Rs4081 RBD mAb[25] (recognizes

quartet 4a but not quartet 4b) was used for detection. Right: ELISA showing detection of both RBD quartets 4a and 4b on the surfaces of eVLPs purified from supernatants of cells co-transfected with mRNAs encoding RBD quartet 4a-EABR and 4b-EABR constructs. The mean absorbance of two replicates is shown as a function of eVLP dilution with error bars representing standard deviations. Binding was not detected for purified supernatant samples from untransfected cells (control) or from supernatants from cells transfected with RBD quartet 4a, RBD quartet 4a-EABR, RBD quartet 4b, RBD quartet 4b-EABR, or RBD quartet 4a plus RBD quartet 4b (all data were plotted but some data points near 0.0 A_{450} are obscured by others).

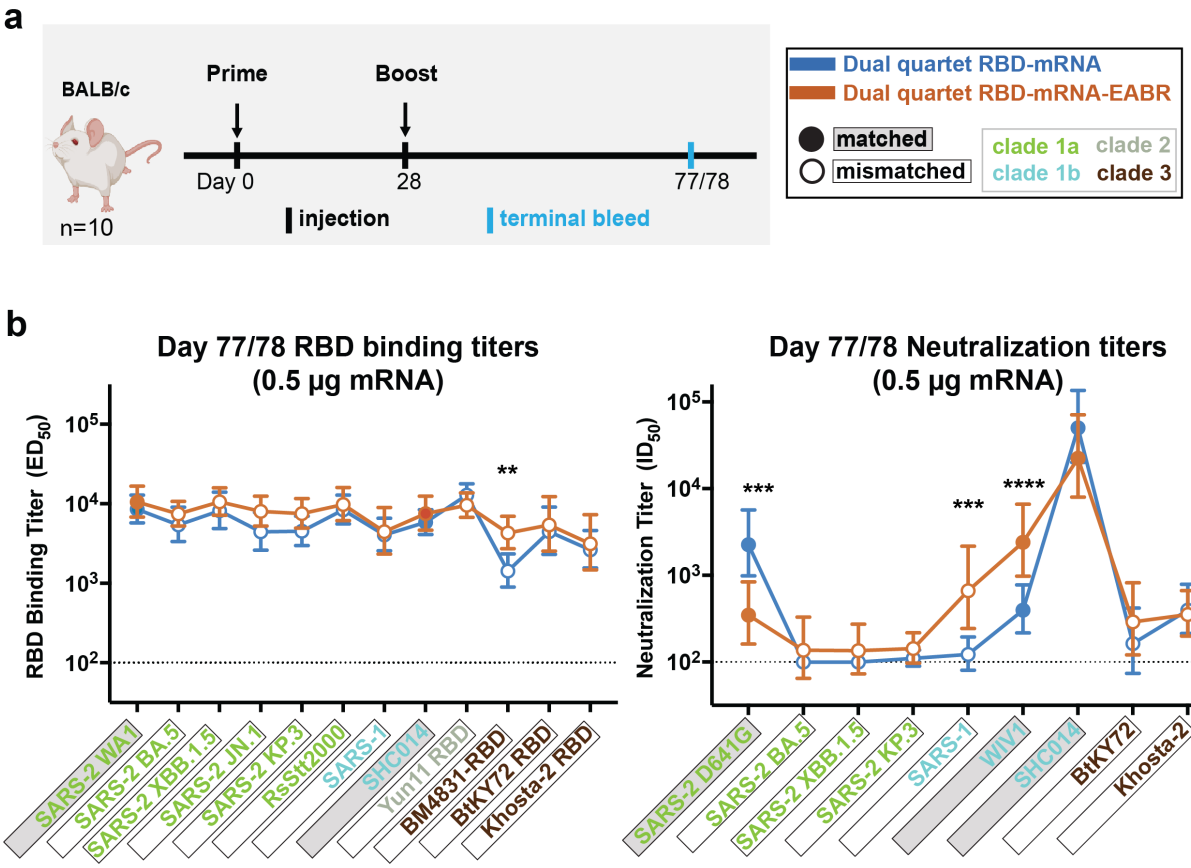

Extended Data Figure 2. Dual quartet mRNAs elicited cross-reactive Abs.
Data are shown for ELISA and neutralization analyses for terminal bleed serum samples (see also Fig. 2). (a) Immunization regimen. Left: Mice were primed at day 0, boosted at day 28, and samples were collected from a terminal bleed at day 77 or 78. Right: Colors used to identify immunizations and symbols indicating a matched (filled in square data points; gray shading around name) or mismatched (unfilled square data points; black outline around name) sarbecovirus antigen. Sarbecovirus strain names are colored in panel b according to clade. (b) RBD-binding ELISA (left) and pseudovirus neutralization (right) results for serum samples from day 77 or 78 after the prime immunization. Immunogens are shown compared with the cohorts immunized with 0.5 µg of an mRNA-based immunogen. Dashed horizontal lines indicate the limits of detection for each assay. Left: Geomeans of ED_{50} values for animals in each cohort (symbols with geometric standard deviations indicated by error bars) are connected by colored lines. Mean titers against RBDs from indicated sarbecoviruses were compared pairwise across immunization cohorts by Tukey's multiple comparison test with the Geisser-Greenhouse correction (as calculated by GraphPad Prism). Right: Neutralization potencies for serum samples from day 77 or 78 after immunization presented as half-maximal inhibitory dilutions (ID_{50} values) of sera against pseudoviruses from the indicated coronavirus strains. Significant differences between the two cohorts are indicated by asterisks: $p<0.05$ = *, $p<0.01$ = **, $p<0.001$ = ***, $p<0.0001$ = ****.

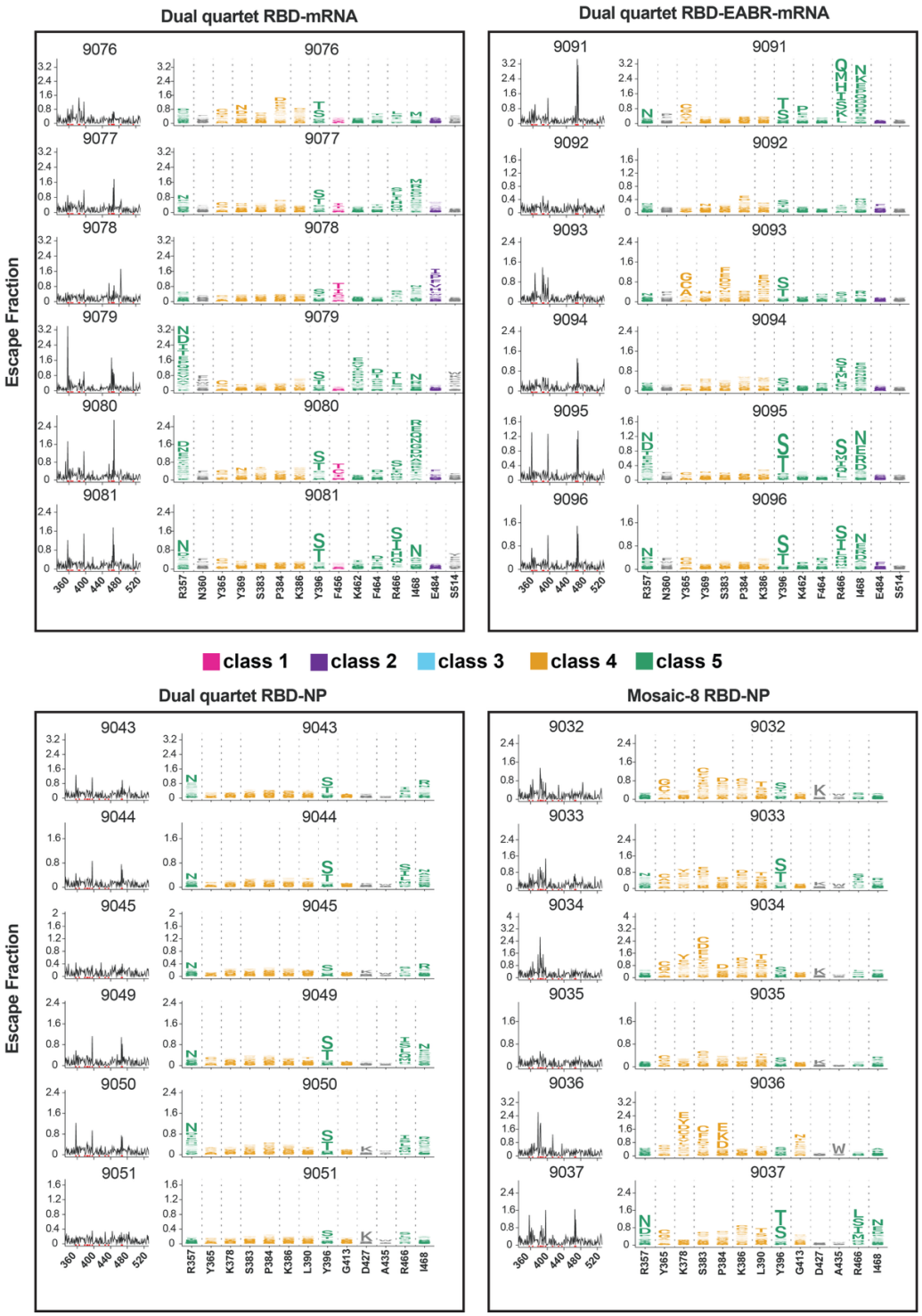

Extended Data Figure 3. DMS line and logo plots (WA1 RBD library) for individual mice. DMS line plots (left) and logo plots (right) for results from individual mice (identified by 4-digit numbers) immunized with the indicated immunogens. X-axes of line and logo plots show RBD residue numbers, and y-axes of line plots show the sum of the Ab escape for all substitutions at an RBD residue (larger numbers indicate increased Ab escape). Sites with the strongest Ab escape are shown in logo plots; tall letters represent the most frequent substitutions at a site. Logo plot residues are colored according to RBD epitopes within different classes[20,44-46] as indicated on the legend.

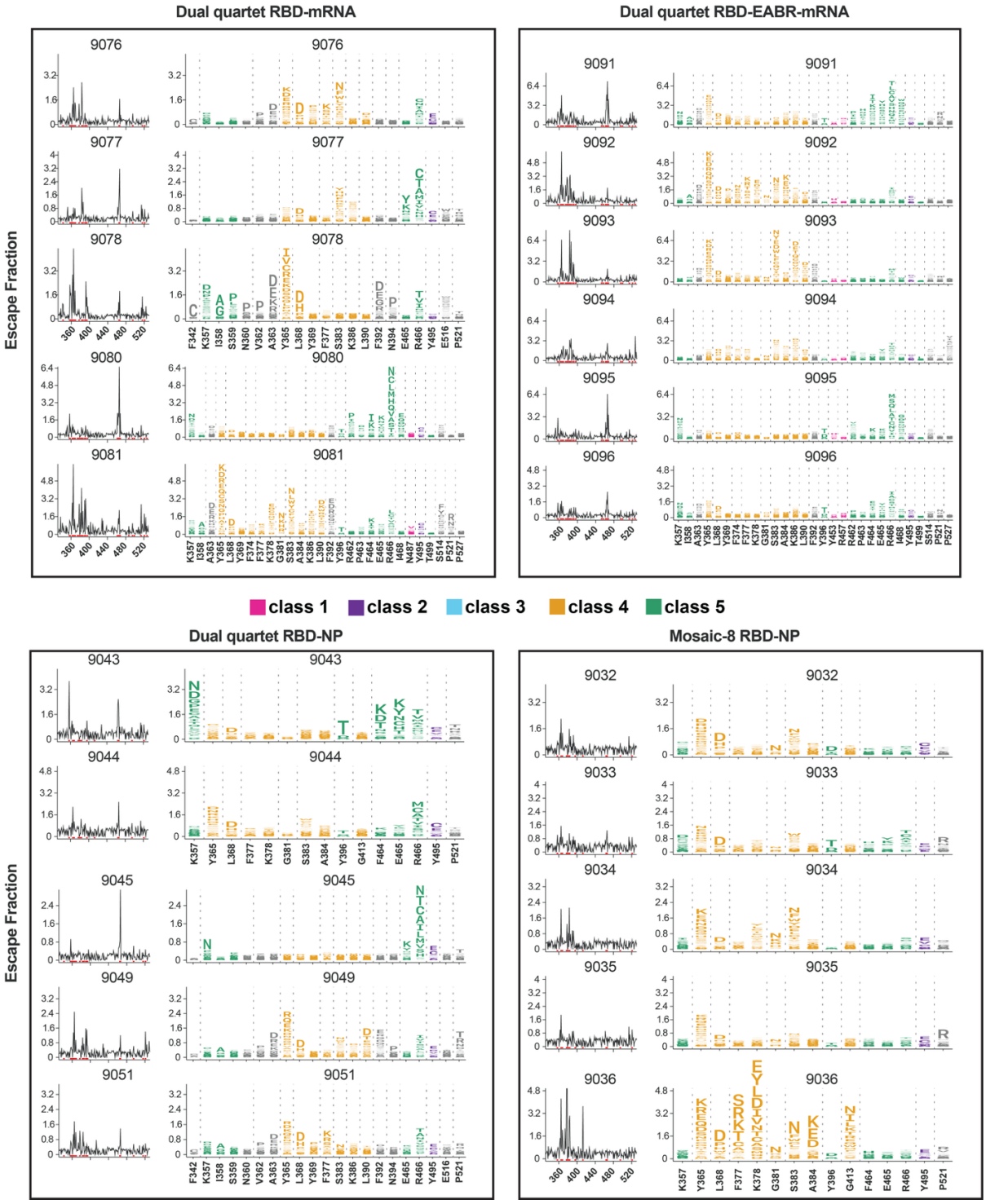

Extended Data Figure 4. DMS line and logo plots (SARS-1 RBD library) for individual mice. DMS line plots (left) and logo plots (right) for results from individual mice (identified by 4-digit numbers) immunized with the indicated immunogens. X-axes of line and logo plots show RBD residue numbers, and y-axes of line plots show the sum of the Ab escape for all substitutions at an RBD residue (larger numbers indicate increased Ab escape). Sites with the strongest Ab escape are shown in logo plots; tall letters represent the most frequent substitutions at a site. Logo plot residues are colored according to RBD epitopes within different classes[20,44-46] as indicated on the legend.

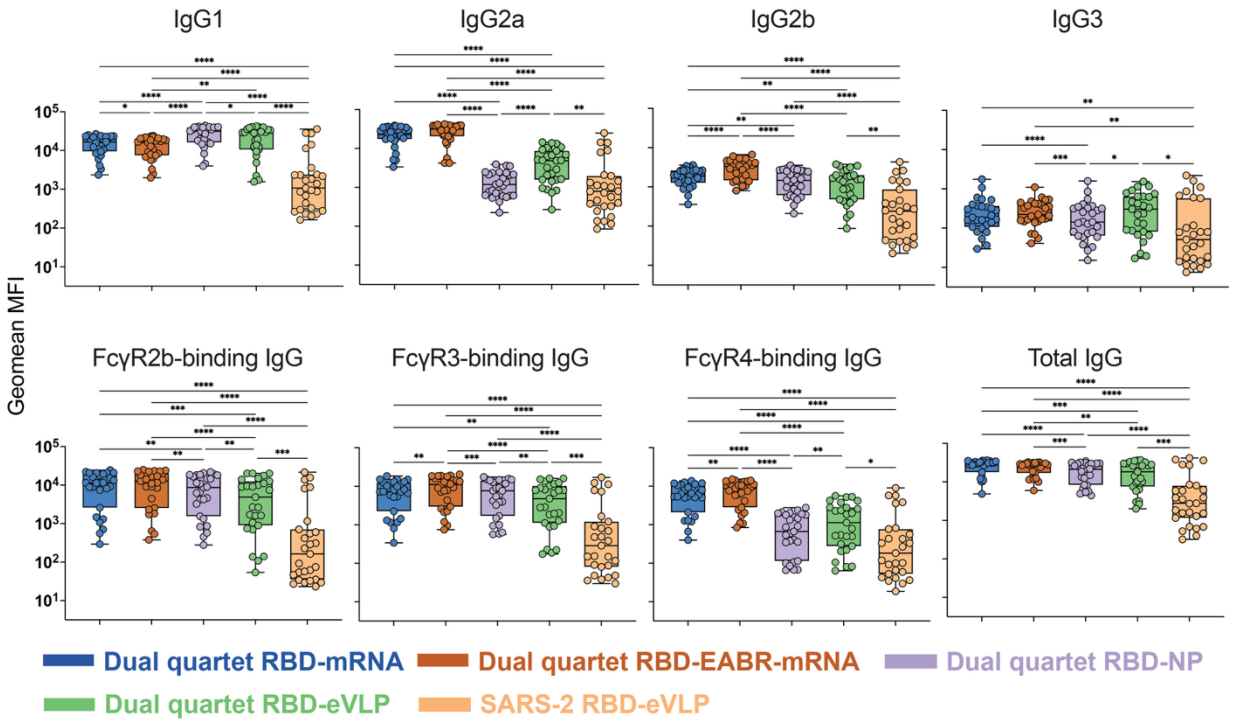

Extended Data Figure 5. mRNA-encoded dual quartet RBD immunogens elicit balanced IgG subclass and potent FcγR-binding responses.

MFI = Median fluorescent intensity. For IgG1, IgG2a, IgG2b, IgG3, FcγR2b-binding IgGs, FcγR3-binding IgGs, FcγR4-binding IgGs, and total IgG, geomean MFI values of the individual responses shown in panel a for each cohort binding to different spikes or RBDs are represented as points in a box and whisker plot and compared pairwise across immunization cohorts by Tukey's multiple comparison test calculated by GraphPad Prism. Significant differences between cohorts linked by vertical lines in panels b and c are indicated by asterisks: $p<0.05$ = *, $p<0.01$ = **, $p<0.001$ = ***, $p<0.0001$ = ****.

See also Fig. 5.

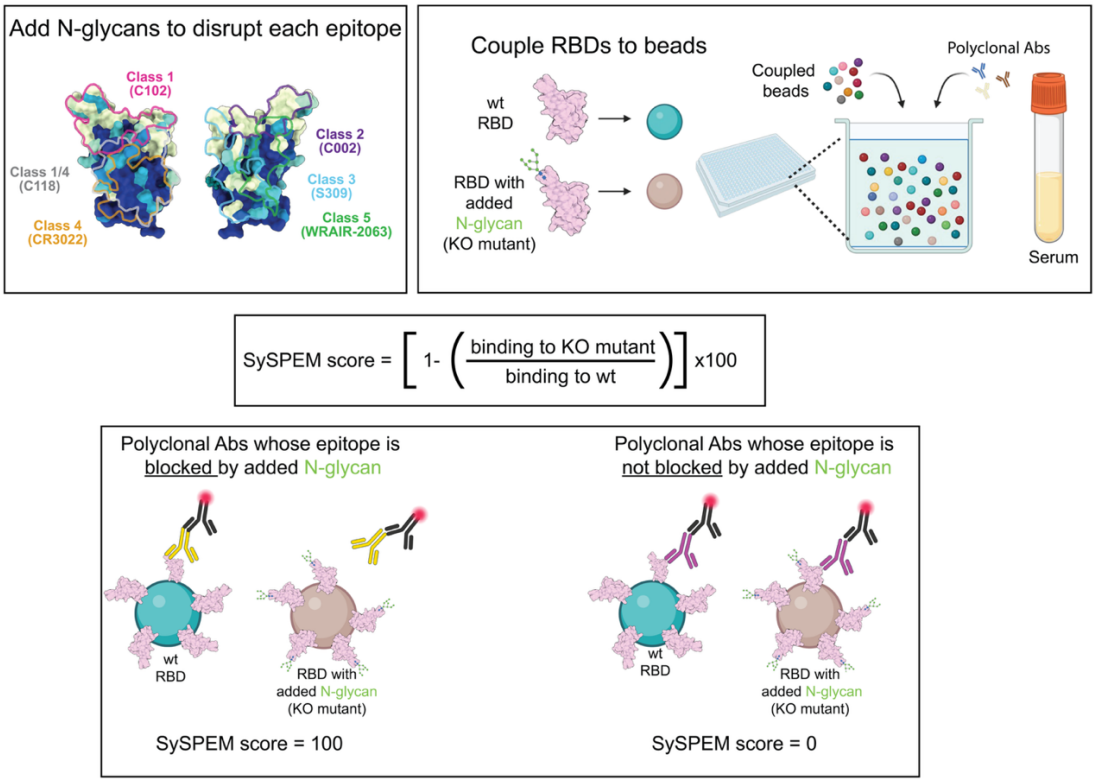

Extended Data Figure 6. Schematic of SySPEM approach.

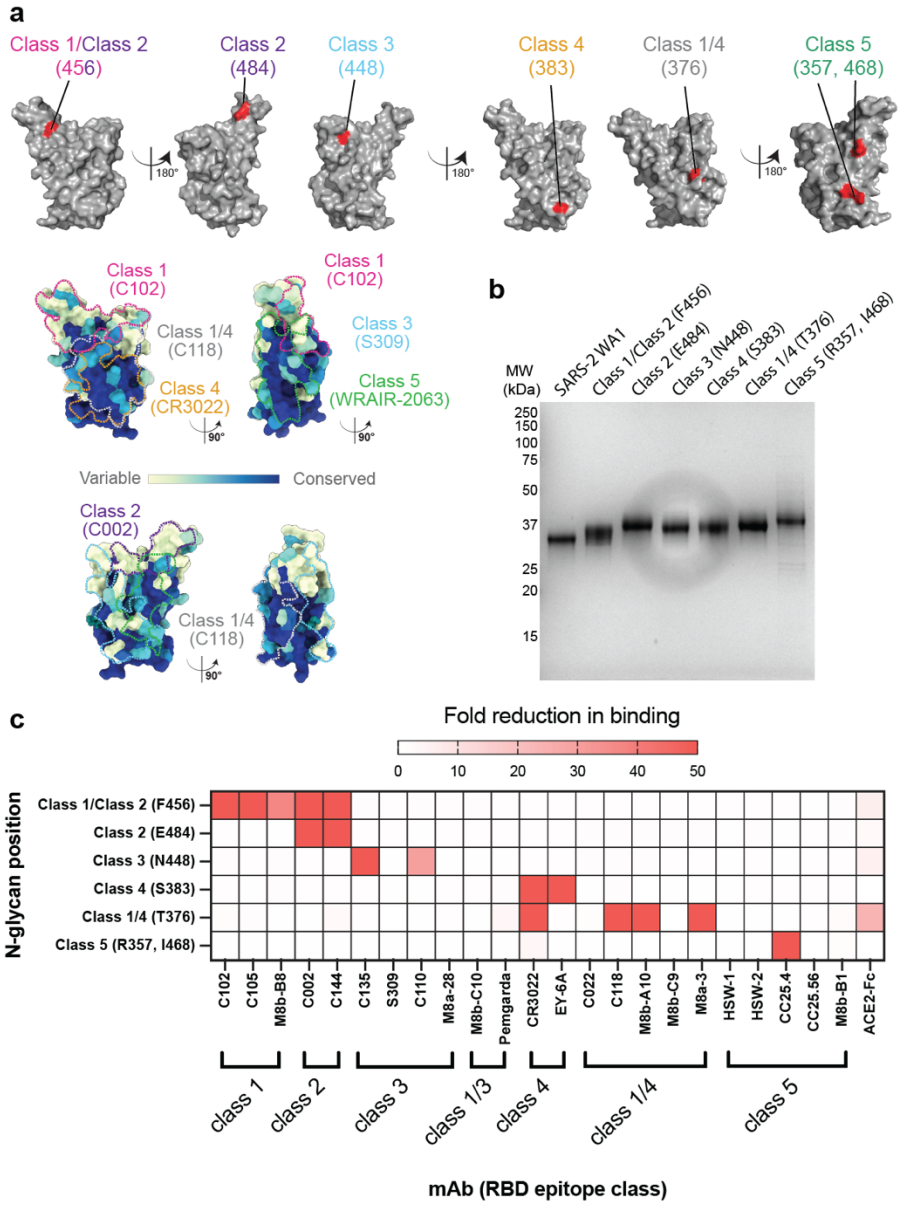

Extended Data Figure 7. Characterization of RBD N-glycan mutants used for SySPEM analysis.

(a) Top: Locations of the added N-glycan(s) in RBD KO mutants, as shown by highlighting of one or more residues that were changed to Asn in the introduced PNGS(s). Bottom: Sequence conservation of 16 sarbecovirus RBDs calculated using ConSurf[48] shown on a surface representation of SARS-2 RBD (PDB 7BZ5). Class 1, 2, 3, 4, 1/4, and 5 anti-RBD Ab epitopes[20,44-46] are outlined in dots in different colors using information from representative structures of Abs bound to SARS-2 spike or RBD (C102: PDB 7K8M; C002: PDB 7K8T, S309: PDB 7JX3; CR3022: PDB 7LOP; C118: PDB 7RKV; WRAIR-2063: PDB 8EOO). (b) SDS-PAGE analysis of purified wt RBD and RBD KO mutants. Molecular weight marker positions are shown on the left with the molecular weight indicated in kilodaltons. KO mutants are listed with the RBD epitope class affected by the N-glycan addition(s) and residue number(s) of Asn residue(s) to which N-linked glycan(s) were added. (c) Results of ELISA showing ratio of binding of characterized mAbs or human ACE2-Fc[20] to wt RBD versus the RBD KO mutants listed on the left. ELISA EC_{50} values for binding of each reagent to wt RBD and the six RBD KO mutants were derived using , and the

fold reduction in binding to each RBD KO mutant was calculated as EC_{50} RBD KO / EC_{50} RBD wt. Classifications of RBD epitopes recognized by the characterized mAbs and ACE-2 Fc are taken from refs[20,25,26,44-46].

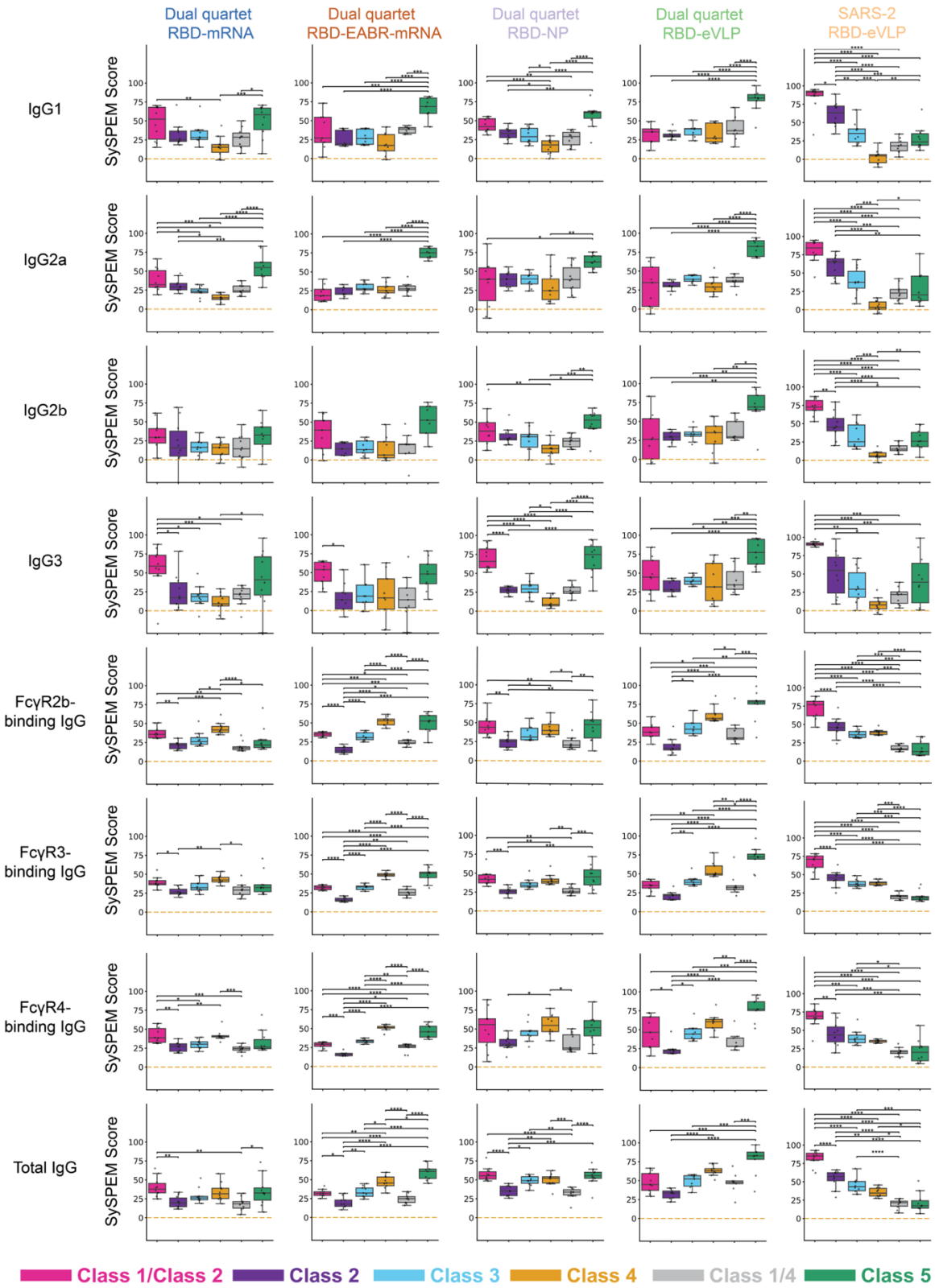

Extended Data Figure 8. SySPEM score comparisons show distinct epitope profiles across immunogen cohorts.

SySPEM scores from individual mice in each immunogen cohort (columns) were determined for each IgG class (rows, IgG subclass plus different FcγR-binding IgGs) with statistical comparisons

between targeted epitopes (colors). A SySPEM value of 0 indicates that none of the IgGs in that sample were affected by the glycan addition and therefore the sample did not contain IgGs that recognize that epitope, and a SySPEM value of 100 indicates that all IgGs in that sample recognized that epitope (Extended Data Fig. 6). A SySPEM value between 0 and 100 indicates the proportion of IgGs in a sample that recognized the epitope that was blocked by glycan addition in the RBD KO mutant. Box and whisker plots of SySPEM scores with individual data points representing one mouse are shown. Significant differences between cohorts were calculated using Tukey's HSD posthoc test and linked by vertical lines indicated by asterisks: $p<0.05$ = *, $p<0.01$ = **, $p<0.001$ = ***, $p<0.0001$ = ****. See also Figs. 6, 7.